LUND UNIVERSITY
Faculty of Science

Quantum ring with tangential dipoles

Carmen López Jurado

Thesis submitted for the degree of Bachelor of Science
Project duration: 2 months (15 hp)

Supervised by Stephanie M.Reimann and co-supervised by Jakob Bengtsson

Department of Physics
Division of Mathematical Physics
May 2021

Abstract

This Bachelor thesis studies the formation of quantum droplets in a dilute dipolar Bose Einstein Condensate with the initial shape of a torus. The main question to address is how this formation occurs as the magnetic dipole moment of the particles changes orientation with respect to the xy plane.
The (mostly) attractive dipolar, and the repulsive contact and Lee-Huang-Yang interactions of the gas are studied first in a theoretical way, and afterwards using a numerical simulation that solves the wave function of the system and computes its ground state energy.
After such study, two main conclusions were drawn. The first one says that independently from the magnetic dipole moment orientation, droplet formation is possible when attractive and repulsive interactions have very similar behaviour, with attraction being slightly stronger than repulsion. Regarding the second one, from all the orientations examined, the one with which droplets have the smallest ground state energy is indeed the xy plane orientation.

Acknowledgements

The first person I would like to thank is my supervisor Stephanie Reimann. She has been very patient, helpful and passionate about this topic. Despite corona, she has been a great supervisor. I would also like to thank Phillip for reviewing this thesis and giving some good advices. To Mikel because without his code, this thesis would have not been possible, and to David, who came up with the idea of tilting the magnetic dipole moments.
Special thanks to my parents, my sister and my brother in law. The have supported me and loved me unconditionally. Thank you so much to Zhanna and Santiago, who have been there in all my ups and downs during my bachelor years. Finally, thank you to my friends from Spain, my physics friends and my corridor mates, each one of them is very special, and make my days more fun.

List of Abbreviations and Acronyms

BEC	Bose-Einstein Condensate
GPe	Gross-Pitaevskii equation
LHY correction	Lee-Huang-Yang correction
BdG	Bogoliubov-de Gennes
LDA	Local Density Approximation

Contents

Chapter 1

Introduction

In 1925, Einstein predicted a phase transition in ideal or non-interacting boson gases [1, 2], based on the paper of Bose [3] about the quantum nature of light. Einstein suggested that due to quantum statistical effects, such transition would occur from a (regular) gas to a new state of matter later called Bose-Einstein condensate (BEC). Below a critical temperature, these ideal boson gases would be in this state in which many of their particles would fall or condense into their ground state; and at 0 K, all particles would condense.
Shortly after, Einstein's and Bose's ideas were brought to more realistic gas models. In 1947, Bogoliubov showed that dilute and therefore weakly interacting gases, i.e. gases whose particles interact pairwise, also condense below a critical temperature. This finding was part of his theory of weakly interacting BECs [4], which, as reviewed in [5], was improved and expanded by Landau, Lifshitz, Penrose and Onsager between 1951 and 1956. It was then the perfect time to start exploring the physical properties resulting from this theory.
In 1938, F. London already suspected that superfluidity, a flow with no loss in kinetic energy that leads to indefinitely rotating vortices or persistent currents, could be a manifestation of ideal bosonic condensation [6]. Thus, it was one of the first properties to be studied. Onsanger (1949) [7] and Feynmann (1955) [8] predicted vortices with quantized angular momentum as a direct consequence of superfluidity. Subsequently, Hall and Vinen (1956) confirmed this idea experimentally [9].
Experiments on dilute BECs did not show up until the seventies, as it was at that time when the necessary experimental techniques started to materialize. All the experimental efforts bore fruit in 1995, when the Bose-Einstein condensation of dilute bosonic gases was realized for the first time by three independent groups [10, 11, 12].
Both before and after this scientific milestone, theoretical physicists continued working on interacting BECs. In the early two-thousands, physicist started to study dilute dipolar gases. The term dipolar refers to gases whose atoms/molecules have a sizable magnetic/electric dipole moment, or a sizable tendency of a magnet (in this case particles) to align with an external magnetic field. During such studies, it was discovered that those magnetic moments are strong enough to give rise to the dipole-dipole interaction, or dipolar interaction.
Coming back to general BEC's, until 2015, it was believed that in dilute interacting BECs, when the attractive interactions were stronger than the repulsive ones, such gases would collapse [13]. In that year, Petrov examined this case for two-component BECs. He suggested that apart from the attractive interspecies interactions and the repulsive intraspecies ones, an additional repulsion, i.e. the Lee-Huang-Yang interaction [14], would overcome the mentioned attraction. In the end, the different forces would be balanced so that stable superfluid quantum droplets would form [15]. Traditionally, the theoretical derivations were done following the mean-field approach, were deviations in the expected value of the energy were discarded. However, Petrov discovered that both those deviations and other terms resulting from the mentioned balance end up having the same size, meaning that the deviations cannot be considered negligible. It is for this reason that the topic of quantum droplet formation was brought relatively late. In 2016, and by accident, quantum droplets were experimentally confirmed in one-component dipolar BECs [16, 17, 18]; and two years later, in two-component non-dipolar BECs [19, 20].
Also in 2018, a new property of BEC's called supersolidity started to be studied. It is a state of quantum many-body systems characterized by both crystalline order (the distinctive feature of solids) and superflu-

idity, and apparently it is related to the interactions among particles. Two competing groups published important works in this field in 2019 [21], and 2020 [22], where supersolidity and quantum droplet formation are discussed in an elongated dipolar BEC and an array of droplets respectively.
Also in 2020, M. N. Tengstrand *et al.* carried on a study [23] in which the mentioned supersolidity, superfluidity and persistent current and droplet formation are examined. They worked with a model of a dilute dipolar BEC of dysprosium atoms confined in a rotating torus. This shape can be realized by magnetoptical trapping techniques, in which an external magnetic field is applied. Therefore, as an additional consequence, the magnetic dipole moments of the system were aligned in the direction of an external magnetic field, which in turn was perpendicular to the torus plane.
According to both the numerical and analytical results obtained, when the system is (practically) in a superfluid state, at an angular momentum L of $N\hbar$, where N is the number of particles being considered, its energy is at a v-shaped minimum with negative curvature. Thus, it is energetically favourable that the gas keeps rotating (persistent current). When the same system is (practically) in the supersolid state, there is a local energy minimum with positive curvature at $L < N\hbar$. There is a vortex in the superfluid part of the condensate, and it is shown that the decay of this state is prevented by a barrier consisting of states where a component of the gas rotates in the opposite direction to that of the vortex. Finally, it was found that the gas might switch from a superfluid to a supersolid state depending on the value of its angular momentum.

David Boholm (one of the authors of [23]) wondered how the mentioned droplet formation, persistent currents and supersolidity would be affected if the dipolar directions were tilted. After private communications, he and Stephanie Reimann (another of the authors of [23] and the supervisor of this thesis) converted this idea into what was meant to be the topic of this Bachelor Thesis.
The first step within this study was set to be a continuation of Boholm's Bachelor thesis [13], where he examined the stabilisation of quantum droplets of a strongly dipolar gas with a quasi-two-dimensional shape. Thus, the first task for this thesis was, by using the physical system in [23], to study the droplet formation for different dipolar orientations while the gas being static.
As it will be further explained in the overview, the first task was completed, but there was no time to rotate the gas. Hence, the topic of this bachelor thesis is just the continuation of [13], with the intention to be continued as planned.

Regarding the structure of this thesis, the second chapter consists of a theoretical background about dipolar BEC's. Ideal BEC's are first introduced as a base for the rest of the theory. Afterwards, the contact and dipole interactions are explained. Subsequently, the differential equation of our system is derived, where a brief a overview of quantum droplet formation is given.
The third chapter is the method. The results of this thesis were generated thanks to a code written by M. N. Tengstrand. Thus, the inputs and outputs of such code are specified, and a general idea about the underlying numerical method is given.
The fourth chapter presents and discusses the results of this thesis. Such results consist of density plots about how quantum droplets form in different dipole orientation scenarios as well as plots showing energy values for each scenario.
Finally, the last chapter is devoted to conclusions and overview, where a recapitulation of everything seen is given, the most important results are summarised, and thesis constraints and possible solutions and expansions are exposed.

Chapter 2

Theory

Einstein adjusted Bose's quantum statistics of light to a more general class of particles nowadays called bosons. This approach took him to the phenomenon that today is known as Bose-Einstein Condensation in ideal gases. As mentioned in the introduction, some theoretical physicists extended the idea of Condensation to interacting bosonic gases afterwards.
In reality BECs are indeed interacting, even the dilute ones, where the characteristic radius of inter-particle interactions is small compared to the mean inter-particle distance [5]. Hence, in this case, interactions involving more than two particles can be considered negligible [5]. Therefore such gases are said to be weakly interacting [1].
The BEC of the system that will be examined not only is dilute, but also dipolar. Thus, the interactions to consider are the contact interaction (which is already present in all interacting gases) the dipole-dipole (or dipolar) interaction, and the Lee-Huang-Yang interaction.
This chapter gives first a brief overview of ideal BEC's, afterwards it introduces the mentioned interactions, and later on, it shows how they are taken into account in the derivation of the differential equation that governs our system.

2.1 Ideal BECs

Bosons is a class of particles in nature. They are indistinguishable, either elementary or composite, either massive or massless, and have integer spin. Photons belong to this class; they are the particles that constitute light, massless and the ones Bose studied.

The Bose-Einstein statistics considers a collection of bosons of the same species. If the particles are non-interacting, the quantum state of the collection as a whole, is a special product, called product state, of the quantum states of any of the particles considered separately. In the context of many-body physics, such separate states are called single-particle states.
Then, this statistics describes how any collection of non-interacting bosons occupy the single-particle states in question.

The following formula is the Bose distribution, which allows determining the expected value for the number of particles occupying the ith single-particle state :

$$\langle n_i(E_i)\rangle = \frac{1}{\exp\left(E_i - \mu\right)/k_b T - 1} \tag{2.1}$$

where E_i is the energy of the ith single-particle state, μ is the chemical potential of the gas, or the energy needed to add one particle into the system, k_b is the Boltzman's constant and T is the temperature of the gas. As it is reviewed in [13], μ cannot be greater than E_0, as the result would be a negative number. Moreover,

[1] It is important to clarify that the term weakly only refers to the fact that in dilute gases, the vast majority of interactions occur pairwise. However, it does not refer to the strength of the (pairwise) interactions themselves.

for low temperatures, the integral over all energies of the distribution tends to zero. Because the integral cannot include the ground state, this can only mean that as the temperature tends to 0 K, more particles form the condensate.
As it will be discussed in more depth, even at low temperatures, interactions make some particles occupy low-lying excited states. This behaviour is not considered in this formula, which would have to be modified if the particle distribution had to be determined.

One of the most important implications of Bose-Einstein statistics is symmetry under particle exchange. That is, if two particles swap their coordinates, the N-body wave function, or the function that describes the state of all the particles as a whole, remains unchanged. This idea can be expressed mathematically in the following way:

$$\psi(\mathbf{r}_1, \mathbf{r}_2, \mathbf{r}_3, ..., \mathbf{r}_i, \mathbf{r}_j, ..., \mathbf{r}_N) = \psi(\mathbf{r}_1, \mathbf{r}_2, \mathbf{r}_3, ..., \mathbf{r}_j, \mathbf{r}_i, ..., \mathbf{r}_N) \tag{2.2}$$

where N denotes the total number of particles in the gas, $\mathbf{r}_n$ denotes nth position, ψ is the N-body wave function and the positions of each parameter in ψ corresponds to a different particle.

Finally, the N-body wave function of an ideal BEC is:

$$\psi(\mathbf{r}_1, ..., \mathbf{r}_N) = \prod_n \phi_0(\mathbf{r}_n) \tag{2.3}$$

where 0 denotes ground-state, and $\phi_0(\mathbf{r}_n)$ is the single-particle ground-state of the nth particle. Eq.(2.3) is said to be symmetrized as it obeys the property of symmetry under particle exchange expressed in Eq.(2.2). It is of importance to mention that this product and all its implications apply to interacting gases as well.

2.2 Dilute dipolar BECs

2.2.1 Contact interaction potential

Bose-Einstein condensation occurs in the ultracold regime (order of nanoKelvin). Even at this low temperature, pairs of particles scatter. Energy-wise, this process is taken into account via a short-range interaction potential [24].
In this ultracold regime, scattering occurs in such a way that the phases of the single-particle wave functions end up shifted. This shifting process is represented by the s-wave scattering length a_s [24], which in turn is proportional to the probability for scattering/interaction [13]. In the case of this thesis, such short-range interaction potential is the following contact interaction potential:

$$V_{con}(\mathbf{r'} - \mathbf{r}) = \frac{4\pi\hbar^2 a_s}{m}\delta(\mathbf{r'} - \mathbf{r}) \equiv g\delta(\mathbf{r'} - \mathbf{r}). \tag{2.4}$$

where $\mathbf{r'}$ and $\mathbf{r}$ are the position vectors of two particles, and $\mathbf{r'} - \mathbf{r}$ is their separation vector.
In 3D, when a_s is positive, as it is the case of this thesis, the interaction is repulsive, whereas when it is negative, the interaction is attractive [24].

2.2.2 Dipole-dipole potential

As mentioned in the introduction, when the atoms/molecules of a dilute gas have a sizable magnetic/electric dipole moment, the dipole-dipole interaction becomes relevant [25].
In our system, the dipolar interaction arises thanks to the magnetic dipole moment of ^{164}Dy atoms (10 μ_B [26]). Moreover, such moments point in the same direction because of an external field that contributes to keeping the gas in a torus shape, as mentioned in the introduction. Thus, the dipole-dipole potential of two particles (see figure 2.1a) is:

$$V_{dd}(\mathbf{r'} - \mathbf{r}) = \frac{\mu_0\mu}{4\pi}\frac{1 - 3\cos^2\theta}{|\mathbf{r'} - \mathbf{r}|^3} \tag{2.5}$$

where μ is the magnetic dipole moment, μ_0 is the permeability of vacuum and θ is the angle between the direction of magnetisation and the separation vector.

Eq.(2.5) is the particular case of formula (2.1) in [25], which shows the dipolar potential for two particles whose electric/magnetic moments are oriented in any direction.

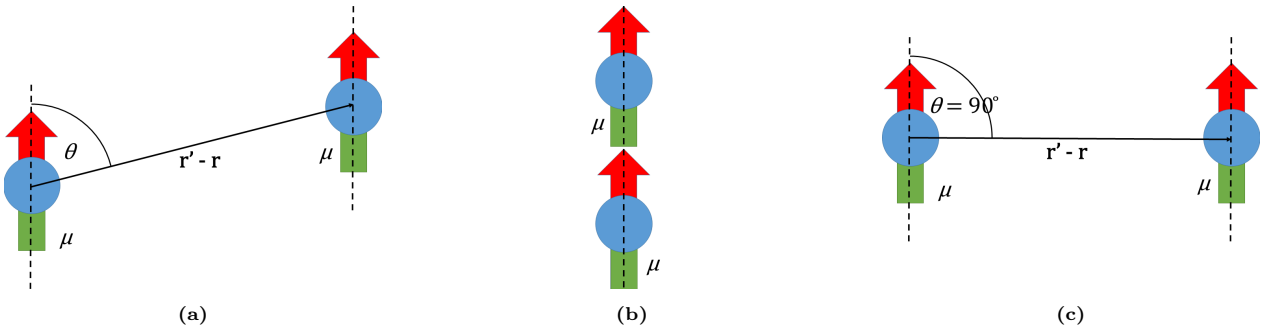

Figure 2.1: Two particles of the same species interacting via dipolar interaction. Both magnetic dipole moments point in the same direction and have magnitude μ. $\mathbf{r}$ and $\mathbf{r'}$ are their position vectors, $\mathbf{r'} - \mathbf{r}$ is their separation vector, and θ is the angle between the direction of magnetization and $\mathbf{r'} - \mathbf{r}$. (a) depicts of the case of $\theta < 90°$. (b) depicts the case of one particle on top of the other, and (c) depicts the case of the two particles in front of each other.

Coming back to Eq.(2.5), and as reviewed in [25], there is a so called *magic angle* ($\theta_m \approx 54.7$) at which the interaction is equal to zero. For angles greater than θ_m, the potential is positive, and therefore the interaction is repulsive. On the other hand, for angles smaller than θ_m, the potential is negative, and therefore the interaction is attractive.
There are two cases that are interesting to examine. The first one consists of one particle right on top of the other (see figure 2.1b). The potential reaches its minimum value, which turns to be negative, so the interaction is attractive at its most. The second case consists of the two particles being side by side (see figure 2.1c). The potential reaches its maximum value, which turns to be positive, so the interaction is repulsive at its most.

The characteristic length of a dipole-dipole interaction a_{dd}, also known as dipolar length, and the relative dipolar strength ϵ_{dd}, are defined as:

$$a_{dd} = \frac{\mu_0 \mu^2 m}{12\pi\hbar^2} \qquad\qquad \epsilon_{dd} = \frac{a_{dd}}{a_s} \tag{2.6}$$

After introducing the contact and dipolar interactions, the full interaction potential of our system is:

$$V_{int}(\mathbf{r'} - \mathbf{r}) = V_{con}(\mathbf{r'} - \mathbf{r}) + V_{dd}(\mathbf{r'} - \mathbf{r}) \tag{2.7}$$

2.2.3 Non-local extended Gross-Pitaevskii equation

The differential equation that governs our system is a non-local extended Gross-Piaevskii equation. Although it can be derived by minimising an integral that represents the energy of the system, this thesis presents an alternative approach, where a temperature of 0 K is assumed.
The derivation of this equation is divided into two parts. In the first one, we reach the non-local Gross-Pitaevskii equation, where quantum fluctuations in energy, i.e. small deviations in the expected value of the energy due to quantum mechanical effects, are considered negligible. In this way, it is possible to apply the Bogoliubov approximation, which allows describing our initial N-body problem in terms of a wave function [27].
In the second part of the derivation, we consider the previously neglected quantum fluctuations. As it was mentioned in the introduction, they are indeed not negligible because of their relative size with respect to the balance between the dipolar and contact interaction energies [15]. Petrov proposed to account for these fluctuations by adding a non-linear term, long ago derived by Lee, Huang, and Yang [14], to the non-local GPe. Afterwards, it was known that in the case of dipolar gases, the term to add is the dipolar Lee-Huang-Yang (LHY) correction [13, 26]. Thus, in the second part of the derivation, we work on the quantum fluctuations

to arrive at the system's actual ground state energy, which in turn leads to the LHY term to include in the non-local GPe.

2.2.3.1 Non-local Gross-Pitaevskii equation

Up to now, we have worked with wave functions. As a reminder, they are functions that assign a complex-valued probability amplitude to every point in space and time. Such output describes the state of the system they represent (one particle in the case of single-particle wave functions, or N particles as a whole for N-body wave functions). To be more precise, when an observable, representing a measurement of a specific property of the system, operates on the wave function, the result is the probability for the system to collapse in a certain state.
However, from now on we will work with fields. Classical fields are functions that assign a tensor to every point in space-time, thus, indicating the value of a property of space-time itself.

One of the main features of the Second Quantization formalism is that fields become operators. The quantum field operators of a BEC are defined as [28]:

$$\hat{\psi}^\dagger(\mathbf{r}) = \sum_{i=0} \phi_i^*(\mathbf{r})\hat{a}_i^\dagger \qquad\qquad \hat{\psi}(\mathbf{r}) = \sum_{i=0} \phi_i(\mathbf{r})\hat{a}_i \tag{2.8}$$

where $\hat{a}_i^\dagger$ and $\hat{a}_i$ are the creation and annihilation operators respectively. They create/annihilate one boson in state i.

The Hamiltonian of a dilute condensate is the sum of a non-interacting (or free) part $\hat{H}_{non-int}$, and an interacting part $\hat{H}_{int}$. $\hat{H}_{non-int}$ contains the kinetic energy and the external potential, while $\hat{H}_{int}$ accounts for the interactions, as its name suggests. Thus, the Hamiltonian we are considering is [24]:

$$\hat{H} = \hat{H}_{non-int} + \hat{H}_{int} = \int d\mathbf{r}\ \hat{\psi}^\dagger(\mathbf{r}) \left[-\frac{\hbar^2}{2m}\nabla^2 + V_{ext}(\mathbf{r})\right] \hat{\psi}(\mathbf{r}) + \frac{1}{2}\int d\mathbf{r'} \int d\mathbf{r}\ \hat{\psi}^\dagger(\mathbf{r})\hat{\psi}(\mathbf{r'})V_{int}(\mathbf{r'}-\mathbf{r})\hat{\psi}(\mathbf{r'})\hat{\psi}^\dagger(\mathbf{r}) \tag{2.9}$$

where m is the mass of the particles,V_{ext} refers to any exterior potential and V_{int} refers to any two-body full interaction potential.

According to the Heisenberg picture, the time derivative of $\hat{\psi}(\mathbf{r},t)$ is:

$$i\hbar\frac{\partial}{\partial t}\hat{\psi}(\mathbf{r},t) = [\hat{\psi}(\mathbf{r},t), \hat{H}] \tag{2.10}$$

By plugging (2.9) into (2.10) and applying the fundamental boson field commutators [28]:

$$[\hat{\psi}(\mathbf{r},t), \hat{\psi}^\dagger(\mathbf{r'},t)] = \delta(\mathbf{r}-\mathbf{r'}) \qquad\qquad [\hat{\psi}(\mathbf{r},t), \hat{\psi}(\mathbf{r'},t)] = 0 \tag{2.11}$$

it is possible to obtain a more explicit time [5]:

$$i\hbar\frac{\partial}{\partial t}\hat{\psi}(\mathbf{r},t) = \left[-\frac{\hbar^2}{2m}\nabla^2 + V_{ext}(\mathbf{r}) + \int d\mathbf{r'}\ \hat{\psi}^\dagger(\mathbf{r'},t)V_{int}(\mathbf{r'}-\mathbf{r})\hat{\psi}(\mathbf{r'},t)\right]\hat{\psi}(\mathbf{r},t) \tag{2.12}$$

In the ultracold regime, and even at 0 K, some of the particles of weakly interacting BECs lie on excited states. As will be explained in depth, this is due to the mentioned quantum fluctuations $\delta\psi(\mathbf{r})$. In this first part of the derivation, the particles lying on the excited states are considered negligible. Such discard allows us to get rid of the terms in (2.8) that do not correspond to the condensate, and finally, to substitute each field operator by a wave function describing the ground state [5, 27]:

$$\hat{\psi}^\dagger(\mathbf{r}) = \phi_0^*(\mathbf{r})\hat{a}_0^\dagger + \sum_{i\neq 0}\phi_i^*(\mathbf{r})\hat{a}_i^\dagger = \phi_0^*(\mathbf{r})\hat{a}_0^\dagger + \cancel{\delta\psi^*(\mathbf{r})} \approx \sqrt{N_0}\phi_0^*(\mathbf{r}) = \psi_0^*(\mathbf{r}) \tag{2.13}$$

$$\hat{\psi}(\mathbf{r}) = \phi_0(\mathbf{r})\hat{a}_0 + \sum_{i\neq 0}\phi_i(\mathbf{r})\hat{a}_i = \phi_0(\mathbf{r})\hat{a}_0 + \cancel{\delta\psi(\mathbf{r})} \approx \sqrt{N_0}\phi_0(\mathbf{r}) = \psi_0(\mathbf{r}) \tag{2.14}$$

where $\hat{a}_0$ and $\hat{a}_0^\dagger$ are replaced by the square of the number of particles in the ground state $\sqrt{N_0}$. This replacement comes from the so-called Bogoliuvob approximation $\langle \hat{a}_0^\dagger, \hat{a}_0 \rangle \approx N_0$, which is valid when $N_0 >> 1$ [5], as it is the case.
Then (2.12) reads:

$$i\hbar\frac{\partial}{\partial t}\psi_0(\mathbf{r},t) = \left[-\frac{\hbar^2}{2m}\nabla^2 + V_{ext}(\mathbf{r}) + \int d\mathbf{r'}\ V_{int}(\mathbf{r'}-\mathbf{r})|\psi_0(\mathbf{r'},t)|^2\right]\psi_0(\mathbf{r},t) \tag{2.15}$$

Finally, after plugging in the interactions taking place in our system according to Eq.(2.7), we obtain

$$i\hbar\frac{\partial}{\partial t}\psi_0(\mathbf{r},t) = \left[-\frac{\hbar^2}{2m}\nabla^2 + V_{ext}(\mathbf{r}) + g|\psi_0(\mathbf{r},t)|^2 + \int d\mathbf{r'}V_{dd}(\mathbf{r'}-\mathbf{r})|\psi_0(\mathbf{r'},t)|^2\right]\psi_0(\mathbf{r},t) \tag{2.16}$$

2.2.3.2 LHY correction

The quantum fluctuations $\delta\psi$ are non-negligible because of the reasons exposed in the introduction and last subsection. They lead to important consequences regarding the description of the condensate.
First, at 0 K, some of the particles lie on single-particle excited states, *depleting* the condensate [26]. It is important to clarify that at higher temperatures, and for both ideal and interacting gases, particles can transit to excited states, this time being thermal fluctuations the reason behind [5]. A second consequence is that the ground state energy has to be corrected [26].
As mentioned before, one can account for these effects by including the dipolar LHY correction to the non-local GPe. There is also an indirect consequence: these quantum fluctuations ultimately lead to an additional repulsion, so that when the dipole interaction is stronger than the contact interaction, it prevents the collapse of the gas. In addition, areas of strong repulsion and attraction are formed, thus, particles accumulate and form quantum droplets with supersolid and superfluid properties.
In this section, we work on those quantum fluctuations to obtain the correction for the ground state. We do so by following Lima and Pelster [26], where they consider a harmonic trapping potential very similar to the one in our system, as it will be seen in 2.2.3.3.

They start from the grand-canonical Hamiltonian $\hat{K} = \hat{H} - \mu\hat{N}$. Here, $\hat{N} = \int d\mathbf{r}\ \hat{\psi}^\dagger(\mathbf{r})\hat{\psi}(\mathbf{r})$ is the operator accounting for the number of particles, and $\hat{H}$ is the Hamiltonian in (2.9), with V_{int} being the sum of the contact interaction in (2.4) and the dipolar interaction corresponding to the case of all dipoles being aligned along the z direction.

The next step is to insert the Bogoliubov prescription $\hat{\psi}(\mathbf{r}) = \psi(\mathbf{r}) + \delta\hat{\psi}(\mathbf{r})$ into $\hat{K}$. Here, $\psi(\mathbf{r})$ is a wave function describing the condensate part, and $\delta\hat{\psi}(\mathbf{r})$ again accounts for the quantum fluctuations. After the insertion, only the resulting terms involving $\delta\hat{\psi}(\mathbf{r})$ being raised to the zeroth, first and second power must be kept .
As a remark, when only the zero-order fluctuation terms are kept, the time-independent GPe is obtained:

$$\mu\psi(\mathbf{r}) = \left[-\frac{\hbar^2}{2m}\nabla^2 + V_{ext}(\mathbf{r}) + g|\psi(\mathbf{r})|^2 + \int d\mathbf{r'}\ V_{dd}(\mathbf{r}-\mathbf{r'})|\psi(\mathbf{r'})|^2\right]\psi(\mathbf{r}) \tag{2.17}$$

Afterwards, and following [29], Lima and Pelster expand the quantum fluctuations :

$$\delta\hat{\psi}(\mathbf{r}) = \sum_\nu{}' \left[U_\nu(\mathbf{r})\hat{\alpha}_\nu + V_\nu^*(\mathbf{r})\hat{\alpha}_\nu^\dagger\right] \tag{2.18}$$

where ν denotes an excited state, also called Bogoliubov mode, the prime denotes that the ground state is discarded, and $U_\nu(\mathbf{r})$ and $V_\nu(\mathbf{r})$ are called the Bogoliubov amplitudes. These amplitudes have to satisfy the following condition:

$$\int d\mathbf{r}\ \left[U_\nu^*(\mathbf{r})U_{\nu'}(\mathbf{r}) - V_\nu^*(\mathbf{r})V_{\nu'}(\mathbf{r})\right] = \delta_{\nu,\nu'} \tag{2.19}$$

as the expansion in (2.18) has to represent a canonical transformation[2].

[2] A canonical transformation is a change of variables in the Hamiltonian of a system such that Hamilton's equations preserve their form when expressed in the new variables.

With the grand-canonical Hamiltonian properly expanded, one would impose its matrix form to be diagonal. As a consequence, one would reach the Bogoliubov de Gennes (BdG) equations:

$$[\epsilon_\nu - H_{FI}(\mathbf{r})]U_\nu(\mathbf{r}) = \int d\mathbf{r'}\ V_{int}(\mathbf{r}-\mathbf{r'})[\psi(\mathbf{r'})\psi(\mathbf{r})V_\nu(\mathbf{r'}) + \psi^*(\mathbf{r'})\psi(\mathbf{r})U_\nu(\mathbf{r'})], \tag{2.20}$$

$$-[\epsilon_\nu + H_{FI}(\mathbf{r})]V_\nu(\mathbf{r}) = \int d\mathbf{r'}\ V_{int}(\mathbf{r}-\mathbf{r'})[\psi^*(\mathbf{r'})\psi^*(\mathbf{r})U_\nu(\mathbf{r'}) + \psi(\mathbf{r'})\psi^*(\mathbf{r})V_\nu(\mathbf{r'})] \tag{2.21}$$

where ϵ_ν is the energy of the excited state ν, and the fluctuation Hamiltonian H_{FI} reads:

$$H_{FI} = -\frac{\hbar^2}{2m}\nabla^2 + V_{ext}(\mathbf{r}) - \mu + \int d\mathbf{r'}\ \psi^*(\mathbf{r'})V_{int}(\mathbf{r}-\mathbf{r'})\psi(\mathbf{r'}) \tag{2.22}$$

After the diagonalization of $\hat{K}$, one would use its ground state $|0\rangle$ to get an expression for the total number of particles in the gas:

$$N = \langle 0|\hat{N}|0\rangle = N_0 + \sum_\nu{}' \int d\mathbf{r}\ V_\nu^*(\mathbf{r})V_\nu^*(\mathbf{r}) \tag{2.23}$$

where the sum is the number of excited particles.

(2.23) is used in the evaluation of the expectation value of $\hat{H}$ to get the general formula for the ground state energy, which reads:

$$E = \int d^3\sqrt{n(\mathbf{r})}\left[-\frac{\hbar^2\nabla^2}{2m} + V_{ext}(\mathbf{r}) + \frac{1}{2}\int d^3V_{int}(\mathbf{r}-\mathbf{r'})n(\mathbf{r'})\right]\sqrt{n(\mathbf{r})} + \Delta E \tag{2.24}$$

with

$$n(\mathbf{r}) = n_0(\mathbf{r}) + \sum_\nu V_\nu^*(\mathbf{r})V_\nu(\mathbf{r}) \tag{2.25}$$

where $n(\mathbf{r})$ is the total number density, or total number of particles per unit of volume, $n_0(\mathbf{r})$ is therefore the condensate density, and ΔE is the mentioned energy shift, which will be determined below. Additionally, the first term of the sum in (2.24) is the ground state energy that would be obtained after applying a method called mean field approximation to Eq.(2.17)

As it is the case of our system, Lima and Pelster are interested in the Thomas-Fermi regime, were the number of particles is large and the kinetic energy of the condensate is negligible in comparison to the interaction energies. Thus, the chemical potential of the time-independent GPe in (2.17) becomes:

$$\mu = \left[V_{ext}(\mathbf{r}) + g|\psi(\mathbf{r})|^2 + \int d\mathbf{r'}\ V_{dd}(\mathbf{r}-\mathbf{r'})|\psi(\mathbf{r'})|^2\right] \tag{2.26}$$

After plugging (2.26) into the BdG equations (2.20) and (2.21), the latter ones reduce to:

$$\left[\epsilon_\nu + \frac{\hbar^2}{2m}\nabla^2\right]U_\nu(\mathbf{r}) = \int d\mathbf{r'}\ V_{int}(\mathbf{r}-\mathbf{r'})[\psi(\mathbf{r'})\psi(\mathbf{r})V_\nu(\mathbf{r'}) + \psi^*(\mathbf{r'})\psi(\mathbf{r})U_\nu(\mathbf{r'})], \tag{2.27}$$

$$-\left[\epsilon_\nu + \frac{\hbar^2}{2m}\nabla^2\right]V_\nu(\mathbf{r}) = \int d\mathbf{r'}\ V_{int}(\mathbf{r}-\mathbf{r'})[\psi^*(\mathbf{r'})\psi^*(\mathbf{r})U_\nu(\mathbf{r'}) + \psi(\mathbf{r'})\psi^*(\mathbf{r})V_\nu(\mathbf{r'})] \tag{2.28}$$

where all the terms in H_{FI} have cancelled each other except from the kinetic term.

One of the two external potentials Lima and Pelster consider is the harmonic trapping potential:

$$V_{tr}(\mathbf{r}) = \frac{m}{2}(w_x^2x^2 + w_y^2y^2 + w_z^2z^2) \tag{2.29}$$

where w_i is the trapping frequency in the ith direction. As it will be explained later, the external potential of our system is indeed a particular case of this harmonic trapping potential.

With the potential (2.29) being dependent on $\mathbf{r}$ in this way, the Bogoliubov amplitudes and ϵ_ν are now "slowly varying functions" of position. This is precisely the condition any function must meet for the so called *semiclassical approximation* to be applied to it. Thus, following the semiclassical approximations in [30] and [31], the new expressions for ϵ_ν, U_ν and V_ν are:

$$\epsilon_\nu \to \epsilon(\mathbf{r},\mathbf{k}) \qquad U_\nu \to U(\mathbf{r},\mathbf{k})e^{i\mathbf{k}\cdot\mathbf{r}} \qquad V_\nu \to V(\mathbf{r},\mathbf{k})e^{i\mathbf{k}\cdot\mathbf{r}} \tag{2.30}$$

where k denotes momentum.
Then, with the substitutions in (2.30), the BdG equations (2.27) and (2.28) become:

$$\left[\epsilon(\mathbf{r},\mathbf{k}) - \frac{\hbar^2\mathbf{k}^2}{2m}\right] U(\mathbf{r},\mathbf{k}) = \sqrt{n_0(\mathbf{r})}\int d\mathbf{r'}\; V_{int}(\mathbf{r}-\mathbf{r'})\sqrt{n_0(\mathbf{r'})}[V(\mathbf{r'},\mathbf{k}) + U(\mathbf{r'},\mathbf{k})]e^{i\mathbf{k}\cdot(\mathbf{r'}-\mathbf{r})}, \tag{2.31}$$

$$-\left[\epsilon(\mathbf{r},\mathbf{k}) - \frac{\hbar^2\mathbf{k}^2}{2m}\right] V(\mathbf{r},\mathbf{k}) = \sqrt{n_0(\mathbf{r})}\int d\mathbf{r'}\; V_{int}(\mathbf{r}-\mathbf{r'})\sqrt{n_0(\mathbf{r'})}[V(\mathbf{r'},\mathbf{k}) + U(\mathbf{r'},\mathbf{k})]e^{i\mathbf{k}\cdot(\mathbf{r'}-\mathbf{r})} \tag{2.32}$$

The last approximation to apply is the Local Density Approximation (LDA). Lima and Pelster use it to derive a non-local term for the non-local interaction between the particles in the condensate and the ones in excited states. Under LDA, the non-local terms in (2.31) and (2.32) of the type:

$$I_{nl}(\mathbf{r},\mathbf{k}) = \sqrt{n_0(\mathbf{r})}\int d\mathbf{r'}\; V_{int}(\mathbf{r}-\mathbf{r'})\sqrt{n_0(\mathbf{r'})}\; q(\mathbf{r'},\mathbf{k})e^{i\mathbf{k}\cdot(\mathbf{r}-\mathbf{r'})} \tag{2.33}$$

where both $U(\mathbf{r},\mathbf{k})$ and $V(\mathbf{r},\mathbf{k})$ are denoted by $q(\mathbf{r},\mathbf{k})$, reduce to:

$$I_{nl}(\mathbf{r},\mathbf{k}) \approx \xi(\mathbf{r},\mathbf{k})q(\mathbf{r},\mathbf{k}) \tag{2.34}$$

with

$$\xi(\mathbf{r},\mathbf{k}) = gn_0(\mathbf{r})[1 + \epsilon_{dd}(3\cos\theta^2) - 1] \tag{2.35}$$

So after plugging (2.34) and (2.35) into (2.31) and (2.32), and performing the proper algebraic manipulations, one would reach the expression for the Bogoliubov amplitudes. In this paper, the expression for V is shown:

$$V^2(\mathbf{r},\mathbf{k}) = \frac{1}{2}\left[\frac{\epsilon_{LDA}(\mathbf{r},\mathbf{k})}{\epsilon(\mathbf{r},\mathbf{k})} - 1\right] \tag{2.36}$$

where ϵ and ϵ_{LDA} are given by:

$$\epsilon^2(\mathbf{r},\mathbf{k}) = \epsilon^2_{LDA}(\mathbf{r},\mathbf{k}) - \xi^2(\mathbf{r},\mathbf{k}) \qquad \epsilon_{LDA}(\mathbf{r},\mathbf{k}) = \frac{\hbar^2\mathbf{k}^2}{2m} + \xi(\mathbf{r},\mathbf{k}) \tag{2.37}$$

Although Lima and Pelster do not specify how, by using (2.36) they finally reach the correction for the ground state:

$$\Delta E(\mathbf{r}) = \frac{64}{15}\; gn(\mathbf{r})^2\sqrt{\frac{n(\mathbf{r})a_g s^3}{\pi}}\; Q_5(\epsilon_{dd}) \tag{2.38}$$

with

$$Q_5(x) = (1-x)^{5/2}\;{}_2F_1\left(-\frac{5}{2},\frac{1}{2};\frac{3}{2};\frac{3x}{x-1}\right) \tag{2.39}$$

where ${}_2F_1$ is the hypergeometric, or Gauss' hypergeometric, function.
$Q_5(\epsilon_{dd})$ represents the dipolar contribution to the energy shift. For $0 \le x \le 1$, it is an increasing function that ranges from 1.0 to 2.6; whereas for $x > 1$, it takes imaginary numbers. In the context of this thesis, $x > 1$ occurs when the dipolar interaction is stronger than the contact interaction. Before Petrov [15], this was taken as a sign of collapse of the gas. Nowadays it is known that ignoring the imaginary part ultimately leads to a good approximation of the experimental data on quantum droplet formation.

According to [13], (2.38) has to be added to the expression for the contact potential, as it is an extra repulsion with which quantum droplet formation is possible; being this what the LHY correction would consist of.

2.2.3.3 Differential equation of the system

The differential equation that governs our system is then [23]:

$$i\hbar\frac{\partial}{\partial t}\psi_0(\mathbf{r},t) = \left[-\frac{\hbar^2}{2m}\nabla^2 + V_{ext}(\mathbf{r}) + g|\psi_0(\mathbf{r},t)|^2 + \int d\mathbf{r'}V_{dd}(\mathbf{r'}-\mathbf{r})|\psi_0(\mathbf{r'},t)|^2 + \gamma|\psi_0(\mathbf{r},t)|^3\right]\psi_0(\mathbf{r},t) \quad (2.40)$$

where, as a recapitulation, the first term in the sum of the right hand side is the kinetic energy; V_{ext} is the external potential, which in our case is the harmonic trapping potential due to the trapping technique used; the third and fourth terms account for the contact and dipole-dipole interactions respectively; and the last term is the LHY correction due to the non-negligible quantum fluctuations in energy.
The expression for V_{ext}, in cylindrical coordinates, is [23]:

$$V_{ext} = V_{trap} = \frac{mw^2}{2}[(\rho-\rho_0)^2 + \lambda^2 z^2] \quad (2.41)$$

where w is the axial trapping frequency and has the value of 2π kHz, ρ_0 is the radius of the torus and has the value of 1 μm, and λ is the ratio of transversal and axial trapping frequencies and has the value of 1.
Finally, the expression for γ is [23]:

$$\gamma = \frac{128\sqrt{\pi}}{3}\frac{\hbar^2 a_s^{5/2}}{m}\left(1+\frac{3}{2}\epsilon_{dd}^2\right) \quad (2.42)$$

where ϵ_{dd} is defined as in Eq.(2.6).

Chapter 3

Method

The differential equation of our system (Eq.(2.40)) cannot be solved analytically. In this thesis, a program has been used, where a split operator imaginary time method [13] that solves such equation, is implemented. In the first section of this chapter, basic information about the input and output of the program is given, as it will be important to understand the remaining chapters better. The second section explains the most important ideas underlying such numerical method.

3.1 Basic information of the program

Given a set of parameters, the program first solves the differential equation. Then, from the solution, it calculates the kinetic, trap, contact, dipole-dipole, total ground-state (which is a sum of the first four mentioned energies) and total ground-state plus rotational energies of the system. It also calculates the angular momentum of the gas and its 3D density distribution.
Originally, the program used to generate such output only after running all the iterations specified as one of the input parameters. It was modified so that the energies were calculated and displayed on the terminal every 100000 iterations to detect convergence in energy as soon as possible.
It is of interest to take a quick look at the input parameters of the program. These are: ϵ_{dd}, the number of imaginary iterations to execute, the initial guess of the potential, the mesh size or the number of density points to compute, the x, y and z projections of the magnetic dipole moment unit vector, and the imaginary step size.

3.2 The numerical method

As said before, the method used relies on imaginary time propagation. Assuming the system to study is governed by Shrödinger's equation, this technique allows to get the (final) ground-state wave function from its homologous one at $t = 0$ as an initial guess. This approach is relevant in this thesis because by performing some changes to its ultimate conclusion (Eq.(3.7)), it is possible to use it for solving the GPe [13, 27].
The first part of this section explains the theoretical foundation of this approach, for which the reference [32] has been followed. The second part briefly explains the mentioned changes to convert such theoretical foundation into a numerical method for the GPe.

3.2.1 Imaginary time propagation: theoretical foundation

The general mathematical expression of the time propagation operator is [33]:

$$\hat{T} = \exp\left(\frac{-it\hat{H}}{\hbar}\right) \tag{3.1}$$

where $\hat{H}$ is the Hamiltonian of the system to study.
By defining the imaginary time as $\tau = it$, it is possible to write (3.1) as:

$$\hat{T} = \exp\left(\frac{-\tau\hat{H}}{\hbar}\right) \tag{3.2}$$

where increasing the value of τ means to move forwards in imaginary time.

The analytical solution of the time-dependent Shrödinger equation is

$$\psi(\vec{r}, t) = \sum_i \exp\left(\frac{-itE_i}{\hbar}\right) c_i \phi_i(\vec{r}) \tag{3.3}$$

where c_i is a constant that does not depend on time, ϕ_i is the ith eiguenfunction of the Hamiltonian, and E_i is its corresponding eiguenvalue.
In imaginary time, Eq.(3.3) reads:

$$\psi(\vec{r}, \tau) = \sum_i \exp\left(\frac{-\tau E_i}{\hbar}\right) c_i \ \phi_i(\vec{r}) \tag{3.4}$$

Following the main idea of this technique, the initial wave function of the system, in imaginary time, is then:

$$\psi(\vec{r}, \tau = 0) = \sum_i c_i \phi_i(\vec{r}) \tag{3.5}$$

to which the time evolution operator must be applied:

$$\psi(\vec{r}, \tau) = \hat{T}(\tau)\psi(\vec{r}, 0) = \sum_i \exp\left(\frac{-\tau E_i}{\hbar}\right) c_i \ \phi_i(\vec{r}) \tag{3.6}$$

where $\hat{H}\phi_i = E_i\phi_i$ has been used.

To get the ground-state wave function of the system, one can apply the properties of the Hamiltonian operator and the exponential function to Eq. (3.6):

- The Hamiltonian is a Hermitian operator, which implies that its eiguenvalues are real and positive. Asuming no degeneracy, the energies of the system follow $E_0 < E_1 < E_2$...
- The function $\exp(-\tau E_i/\hbar)$ decays more rapidly as E_i increases.

then, the following approximation can be made [33]:

$$\lim_{\tau\to\infty} \psi(\vec{r}, \tau) \approx \exp\left(\frac{-\tau E_0}{\hbar}\right) c_0 \ \phi_0(\vec{r}) = \psi_0(\vec{r}) \tag{3.7}$$

where the non-ground-state terms in the expansion of $\psi(\vec{r}, \tau)$ become negligible when compared to the ground-state term.
Thus, the usage of Eq. (3.7) can be expressed in the following alternative way: it is possible to get the ground-state wave function of a system after its convergence (in energy in the case of this thesis) by applying the time propagation operator to its initial ground-state wave function, which in the case of Shrödinger's equation it turns to be stationary.

3.2.2 Imaginary time propagation: expansion of the time propagation operator

In reality, there is not infinite time, which means that the application of the operator to the initial wave function must be done in a discrete way and for a certain number of imaginary iterations. This can be achieved by using a relatively manageable power series expansion of the Hamiltonian, applying the operator repeatedly and for a small time $\Delta\tau$, and in each application, minimizing the ground-state energy and updating the wave function accordingly.

The Hamiltonian of a particle rotating in a harmonic oscillator trap has a well-known expansion. To use it for solving the GPe, one would need to add terms accounting for the interactions and the LHY correction to it [13]. Then, our time propagator operator is splitted in the following way [13]:

$$e^{-\tau \hat{H}} = e^{-\frac{1}{6}\tau V_{eff}} e^{-\frac{1}{2}\tau T} e^{-\frac{2}{3}\tau \tilde{U}} e^{-\frac{1}{6}\tau V_{eff}} \tag{3.8}$$

where $\tilde{U}$ is an operator related to the potential of the rotating particle system, V_{eff} is an effective potential and T is the kinetic energy of the of the rotating particle system.

T reads in the following way:

$$T = \frac{1}{2}\left[(p_x + \Omega y)^2 + (p_y + \Omega y)^2\right] = \frac{1}{2}\left(T_x + T_y\right) \tag{3.9}$$

where Ω is the rotation momentum strength .
It can be seen that the kinetic energy has the form of a Harmonic Oscillator Hamiltonian, so its corresponding term in can be expanded as well in the following way [34, 13]:

$$e^{-\frac{1}{2}\tau T} = e^{-\tau \frac{1}{2}(T_x + T_y)} = e^{\frac{1}{2}C_v T_x} e^{\frac{1}{2}C_t T_y} e^{\frac{1}{2}C_v T_x} \tag{3.10}$$

Every member of the expression can be represented by a matrix, as they are all operators. By comparing the matrix elements of the LHS with the ones in the RHS, it is possible to determine C_v and C_t:

$$C_v = \frac{\cosh \Omega\tau - 1}{\Omega\tau \sinh \Omega\tau} \qquad\qquad C_t = \frac{\sinh \Omega\tau}{\Omega\tau} \tag{3.11}$$

In our study the gas is static, thus, it is necessary to expand both expressions as Ω is in their denominator. Because the smaller $\Delta\tau$ is , the more accurate the final wave function will be, it is correct and even needed to use the expansions of C_v and C_t for $\tau \to 0$ [35]:

$$C_v = \frac{1}{2} - \frac{1}{24}\Omega^2\tau^2 + \frac{1}{240}\Omega^4\tau^4 + ... \qquad\qquad C_t = 1 + \frac{1}{6}\Omega^2\tau^2 + \frac{1}{120}\Omega^4\tau^4 + ... \tag{3.12}$$

so we will take $C_v = \frac{1}{2}$ and $C_t = 1$.

Finally, V_{eff} reads in the following way: [13]:

$$V_{eff} = V_{ext} + V_{con} + V_{dd} - \frac{1}{2}\Omega(\hat{x}^2 + \hat{y}^2) + LHY \tag{3.13}$$

where V_{con} is the contact potential in (2.4), V_{dd} is the dipolar potential in (2.5) and this case V_{ext} is the harmonic oscillator trap. Reference [13] explains in a detailed way how to add the LHY-correction, which here it is denoted as LHY, to this potential.

Chapter 4

Results and discussion

This chapter shows and discusses the density plots and energy data obtained from the solutions of the equation of our system (2.40). We first focus on the shape of the gas; afterwards, we relate such shapes with the dipole and contact energies of the system, where in the latter, the LHY contribution is included; and finally, we discuss the kinetic and ground-state energies in more general terms.

4.1 Droplet formation

Density plots allowed the study of the shape of the gas. Each one of them corresponds to a different magnetic dipole moment orientation and ϵ_{dd} value. The orientations considered in this thesis are z axis, about 67.5°, 45° and 22.5° from the xy plane, and on the xy plane per se.
All the results were generated by using a mesh size of 2^7, an imaginary step size of 0.005, and contour densities $0.8 \cdot 10^{-3}, 0.4 \cdot 10^{-3}$ and $0.1 \cdot 10^{-3}$.
In the annexe, density plots are organised by orientation, but in this discussion, they are grouped by shape stages to understand the droplet formation process better.

4.1.1 Pancake phase

As figure 4.1 shows, at $\epsilon_{dd} = 0.45$ and for all orientations, the gas takes the form of a thick pancake, its density is low and seems to be uniform. These two observations might result from the repulsive contact interaction being 2.22 times stronger than the dipolar interaction and not depending on any angle θ.

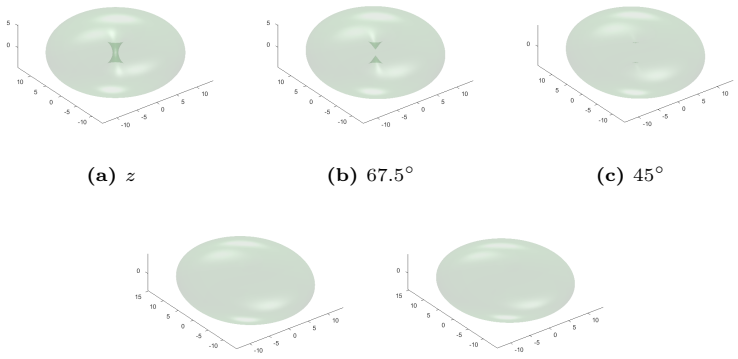

(a) z **(b)** 67.5° **(c)** 45°

(d) 22.5° **(e)** xy

Figure 4.1: Gas density plots that correspond to the pancake phase for all orientations, where $\epsilon_{dd} = 0.45$.

4.1.2 Tori phase

For orientations z and 67.5°, this tori phase occurs between $\epsilon_{dd} = 0.90$ and $\epsilon_{dd} = 0.95$. The corresponding density plots are shown in figure 4.2 (first row for z orientation and second row for 67.5°), where the gas evolves into first one torus of very small inner radius ($\epsilon_{dd} = 0.90$), then into two concentric tori where the inner one is denser than the outer one ($\epsilon_{dd} = 1.45$ and $\epsilon_{dd} = 1.90$), and finally into three concentric tori, where again the innermost one is the densest ($\epsilon_{dd} = 1.95$).

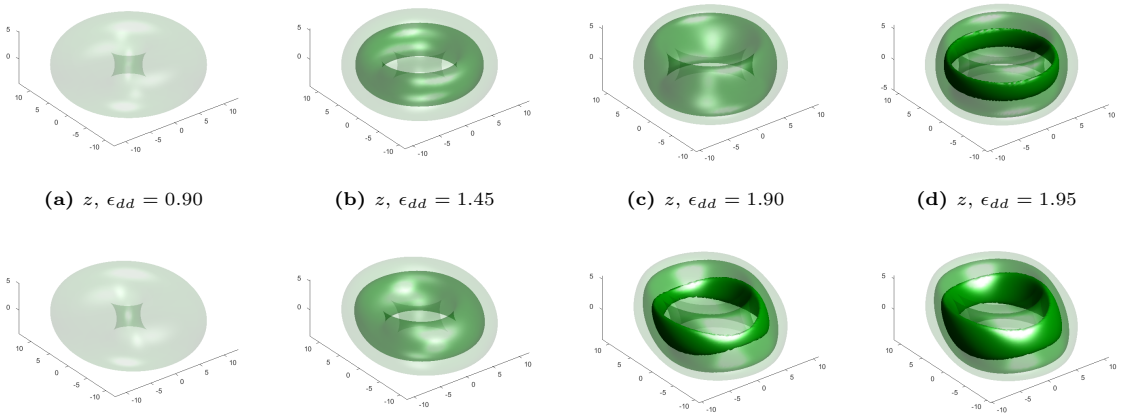

(a) z, $\epsilon_{dd} = 0.90$ **(b)** z, $\epsilon_{dd} = 1.45$ **(c)** z, $\epsilon_{dd} = 1.90$ **(d)** z, $\epsilon_{dd} = 1.95$

(e) 67.5°, $\epsilon_{dd} = 0.90$ **(f)** 67.5°, $\epsilon_{dd} = 1.45$ **(g)** 67.5°, $\epsilon_{dd} = 1.90$ **(h)** 67.5°, $\epsilon_{dd} = 1.95$

Figure 4.2: Gas density plots that correspond to the tori phase for orientations z (first row), and 67.5° (second row). In both cases, ϵ_{dd} increases from 0.90 to 1.95.

Figure 4.3 contains the density plots that correspond to the tori phase for orientations 45°, 22.5° and xy.This time such phase consists of only two concentric tori, at $\epsilon_{dd} = 0.90$ and 1.45 in the case of 45° (subfigures 4.2a and 4.2b), and at $\epsilon_{dd} = 0.90$ in the case of 22.5° (subfigure 4.3c) and xy (subfigure 4.3d).

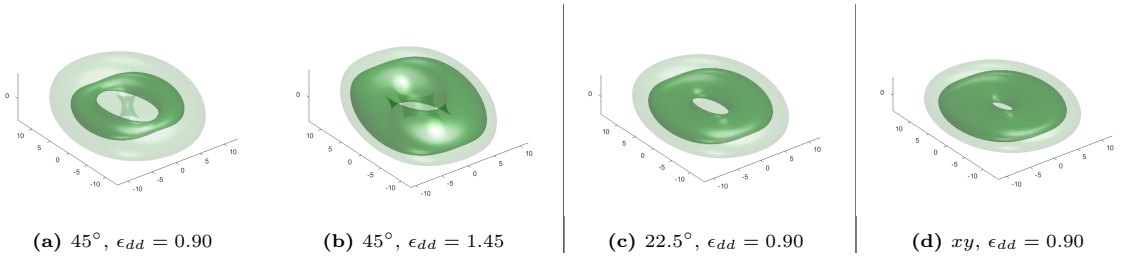

(a) 45°, $\epsilon_{dd} = 0.90$ **(b)** 45°, $\epsilon_{dd} = 1.45$ **(c)** 22.5°, $\epsilon_{dd} = 0.90$ **(d)** xy, $\epsilon_{dd} = 0.90$

Figure 4.3: Gas density plots that correspond to the tori phase for orientations 45° (subfigures 4.3a and 4.3b), 22.5° (4.3c) and xy (4.3d).

Notice that in general, as ϵ_{dd} increases, so does the thickness of the tori in the dipole orientations. This might be an early hint about droplet formation occurring in the direction of magnetisation, as it will be further discussed.
Notice as well, that as the orientation of the dipoles approaches the xy plane, the concentric-tori substage occurs before and last shorter in terms of ϵ_{dd}. This might be another early hint, this time suggesting that as the orientation approaches the xy plane, droplets become more evident before.

Regarding the density of the concentric tori, a first reason why the inner tori are denser than the outer ones might be the $1/|\mathbf{r'} - \mathbf{r}|^3$ dependance of the dipole interaction, thus penalising distance even more rapidly than the contact interaction. A second reason could be that from the previous phase, the further particles are

from the inner zone, the fewer neighbouring particles they can interact with, and this becomes more evident as the dipolar interaction becomes stronger.

4.1.3 Intermediate phase

Orientations 45°, 22.5° and xy seem to have an intermediate stage prior to quantum droplets being fully noticeable. It occurs at $\epsilon_{dd} = 1.90$ and 1.95 for the orientation 45°, and at $\epsilon_{dd} = 1.45$ for 22.5° and xy. The density plots of this phase are shown in figure 4.4 (subfigures 4.4a and 4.4b for 45°, subfigure 4.4c for 45°, and subfigure 4.4d for xy), where there are two droplets in front of each other, both being embraced by the before mentioned innermost torus. Thus, this phase may be first, a manifestation of side by side dipoles repelling to each other, and second, an early hint about the shape of the droplets at the next and last phase (droplet differentiation) for such orientations, as it will be discussed.

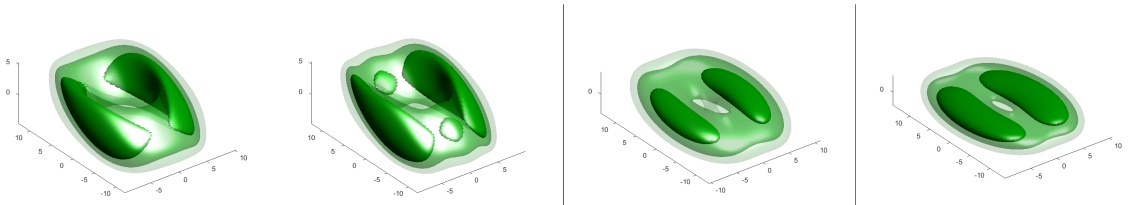

(a) 45°, $\epsilon_{dd} = 1.90$ **(b)** 45°, $\epsilon_{dd} = 1.95$ **(c)** 22.5°, $\epsilon_{dd} = 1.45$ **(d)** xy, $\epsilon_{dd} = 1.45$

Figure 4.4: Gas density plots that correspond to the intermediate phase for orientations 45° (subfigures 4.4a and 4.4b), 22.5° (4.4c) and xy (4.4d).

4.1.4 Droplet differentiation phase

For orientations z and 67.5°, this last phase occurs at $\epsilon_{dd} = 2.03$. Figure 4.5 contains the corresponding density plots, with the first row for z orientation, and second row for 67.5°.
In the case of z orientation, the gas has eight droplets at $\epsilon_{dd} = 2.03$ (subfigure 4.5a), and seven for the rest of ϵ_{dd} values; whereas in the case of 67.5°, the gas has eight droplets from $\epsilon_{dd} = 2.03$ to $\epsilon_{dd} = 2.12$ (subfigures 4.5e to 4.5g), and six figures at $\epsilon_{dd} = 2.18$ (subfigure 4.5h). This decrease in droplet number seems to occur in such a way that droplets from the leftmost and right most part merge with themselves respectively.

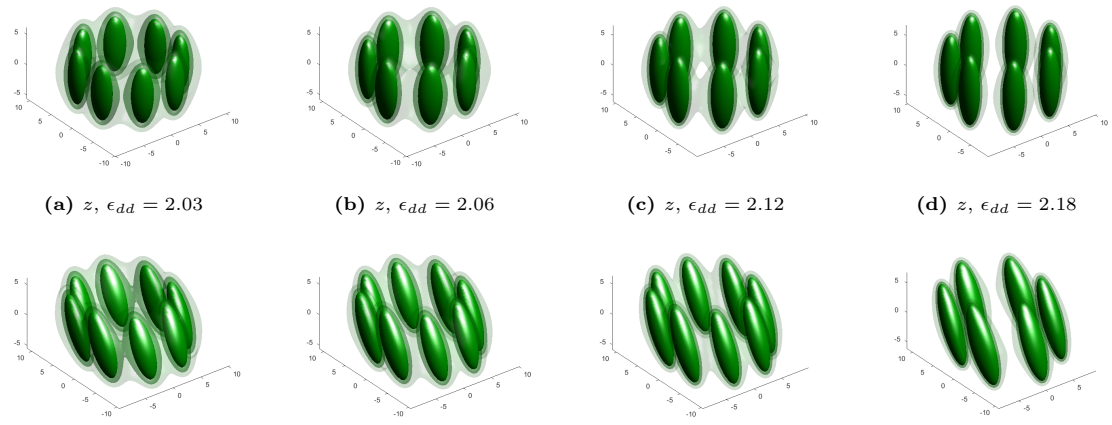

(a) z, $\epsilon_{dd} = 2.03$ **(b)** z, $\epsilon_{dd} = 2.06$ **(c)** z, $\epsilon_{dd} = 2.12$ **(d)** z, $\epsilon_{dd} = 2.18$

(e) 67.5°, $\epsilon_{dd} = 2.03$ **(f)** 67.5°, $\epsilon_{dd} = 2.06$ **(g)** 67.5°, $\epsilon_{dd} = 2.12$ **(h)** 67.5°, $\epsilon_{dd} = 2.18$

Figure 4.5: Gas density plots that correspond to the droplet differentiation phase for orientations z (first row), and 67.5°. At both rows, ϵ_{dd} increases from $\epsilon_{dd} = 2.03$ to $\epsilon_{dd} = 2.18$.

Figure 4.6 shows the density plots that correspond to the differentiation phase for orientation 45°, which starts at $\epsilon_{dd} = 2.03$ as well. As it can be seen, the two lateral droplets from the intermediate stage (subfigures 4.4a and 4.4b) continue being noticeable until $\epsilon_{dd} = 2.12$ (subfigure 4.6c), and by $\epsilon_{dd} = 2.18$, they have separated into two droplets.

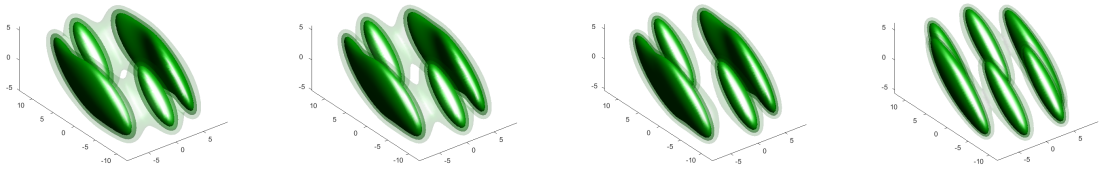

(a) 45°, $\epsilon_{dd} = 2.03$ **(b)** 45°, $\epsilon_{dd} = 2.06$ **(c)** 45°, $\epsilon_{dd} = 2.12$ **(d)** 45°, $\epsilon_{dd} = 2.18$

Figure 4.6: Gas density plots that correspond to the droplet differentiation phase for orientation 45°, where ϵ_{dd} increases from $\epsilon_{dd} = 2.03$ to $\epsilon_{dd} = 2.18$.

For orientations 22.5° and xy, this phase starts at $\epsilon_{dd} = 1.90$. The corresponding plots are shown in figure 4.7, where the first two rows corresponds to orientation 22.5° and the last one to xy. In figures 4.5 and 4.6 there seems to be a tendency of droplets merging side-by-side, and could be considered an anticipation of the two well differentiated droplets that one can see in this last figure.

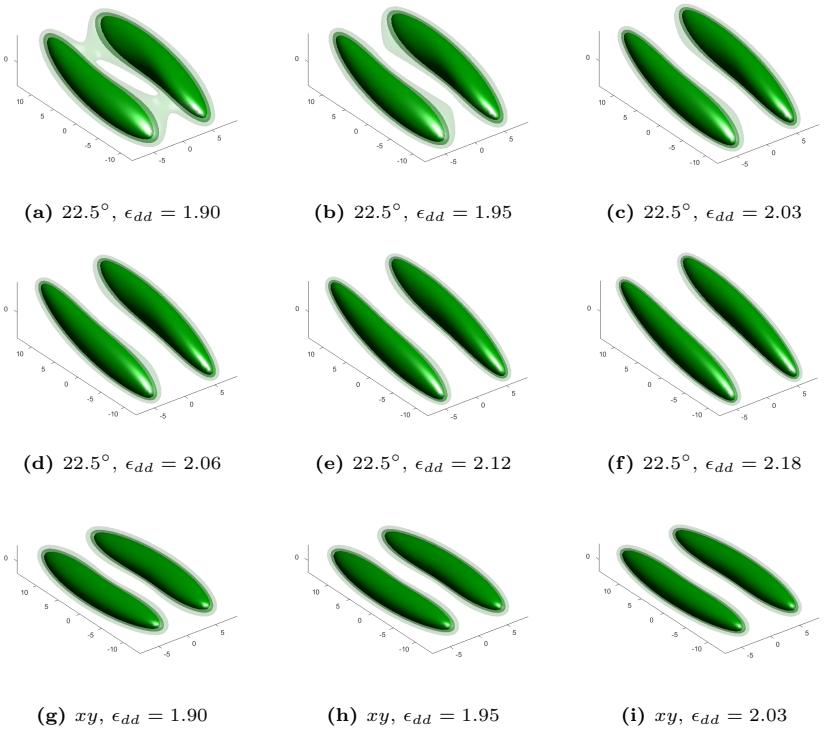

(a) 22.5°, $\epsilon_{dd} = 1.90$ **(b)** 22.5°, $\epsilon_{dd} = 1.95$ **(c)** 22.5°, $\epsilon_{dd} = 2.03$

(d) 22.5°, $\epsilon_{dd} = 2.06$ **(e)** 22.5°, $\epsilon_{dd} = 2.12$ **(f)** 22.5°, $\epsilon_{dd} = 2.18$

(g) xy, $\epsilon_{dd} = 1.90$ **(h)** xy, $\epsilon_{dd} = 1.95$ **(i)** xy, $\epsilon_{dd} = 2.03$

Figure 4.7: Gas density plots that correspond to the droplet differentiation phase for orientations 67.5° (first two rows), where ϵ_{dd} increases from 1.90 to 2.18; and xy (last row), where ϵ_{dd} increases from 1.90 to 2.03

4.2 Energies of the system

To understand the droplet formation in great detail, it is necessary to expand the explanations in the previous section with a discussion about the system's energies. This subsection shows plots of different energies of the system, where each data point corresponds to an orientation and ϵ_{dd} values considered in this thesis.

4.2.1 Dipolar interaction energy

Figure 4.8 shows the dipolar interaction energy of the gas. The general trend consists of the dipolar interaction energy becoming more negative as ϵ_{dd} increases. According to the theory, the more negative the dipolar interaction is, the more particle attraction there is in some regions of space. Thus, the mentioned trend seems to be consistent with the quantum droplet formation seen in the previous section (4.1), with the gas evolving from a thick pancake shape to more defined and elongated droplets.

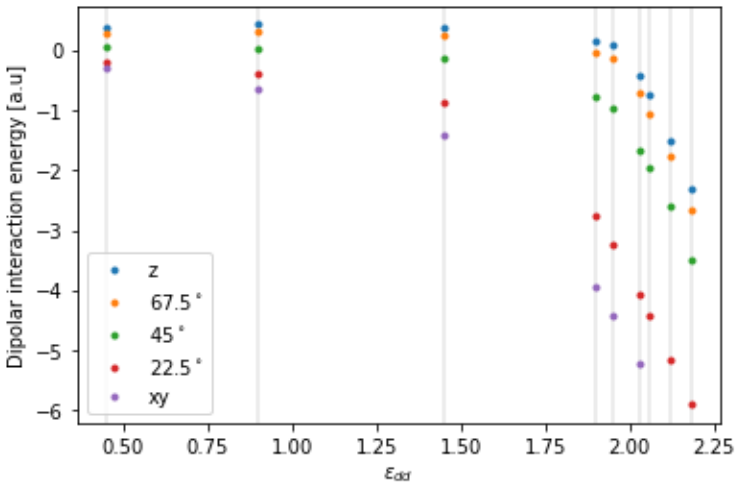

Figure 4.8: Dipolar interaction energy vs ϵ_{dd} for all subfigures.

Per every orientation, there seem to be two different decreasing slopes, such that the fastest one occurs at high values of ϵ_{dd}.
More precisely, for orientations z and 67.5°, this fast slope seems to start at $\epsilon_{dd} = 2.03$, coinciding with the beginning of the droplet differentiation phase (see 4.5). In the case of 45°, it seems to start at $\epsilon_{dd} = 1.95$, coinciding with the last substage of the intermediate phase (see 4.4b). Finally, for orientations 22.5° and xy, it seems to do so at $\epsilon_{dd} = 1.90$, again coinciding with the beginning of the droplet differentiation phase (see 4.6). Regarding the slow slopes, they appear to become steaper as the orientation approaches the xy plane. All this suggests that the attractive dipolar interaction is crucial for droplets to become better defined, as the mentioned ϵ_{dd} values and the modulus of the slowest slopes are consistent with the observation in the previous section about droplets becoming evident earlier as the orientation approaches the xy plane.
There is a last and interesting remark concerning the slopes. It seems that all fast slopes have the same modulus. This could mean that at least for the dipolar interaction energy, the droplet differentiation mechanism is the same regardless of the orientation of the dipoles.

Finally, the data points seem to cluster by orientation. The ones for orientations z and 67.5° are quite close to each other. The values for 45° are a bit separated from the ones for 67.5° , but still seem to also belong to this first cluster. A second cluster is composed by the energy values of the orientations 22.5°, xy, which seem to be separated in the same way as well.

4.2.2 Contact interaction energy

According to theory, droplet formation is only possible thanks to both particle attraction in some areas of space, and particle repulsion in some other areas. Given that droplet formation has occurred (figures 4.5, 4.6 and 4.7), the conclusions in the previous subsection can be considered correct only if the contact energy in figure 4.9b, which as previously said, includes the LHY repulsion, suitably complements the behaviour discussed in figure 4.8

By comparing the dipolar and contact interaction energies in figures 4.8 and 4.9b, or figures 4.9a and 4.9b, one can notice that for all orientations, both graphs are quite symmetric, if not totally symmetric, with respect to each other. More precisely, both graphs have the following similarities:

- Their general trends consist of the interaction energy in question becoming stronger as ϵ_{dd} increases.
- While in figure 4.9a there seem to be two decreasing slopes per orientation, in figure 4.9b there seem to be two increasing ones. However, this idea about the same fast slope for all orientations, coinciding with stages at which droplets are better defined, applies for 4.9b as well. Moreover, the moduli of such two fast slopes appear to be the same, meaning that also for the contact interaction, the droplet formation mechanism might be the same regardless of the orientation.
- Clustering of data points occurs in the same way.
- Analysing the energy values orientation-wise, from closer to further from zero, or from lower to higher interaction strength, the order is: z - 67.5° - 45° - 22.5° - xy.

Hence, this symmetry allows one to apply the opposite ideas as in the discussion of figure 4.8 for the phenomenon of repulsion.

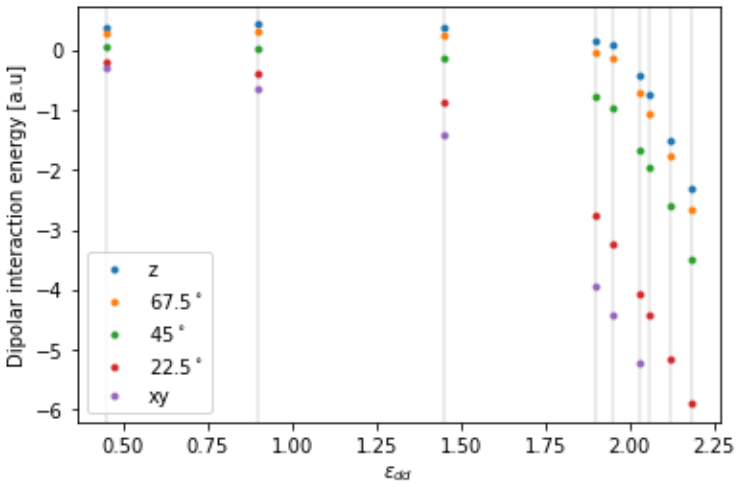

(a) Dipolar interaction energy vs ϵ_{dd}

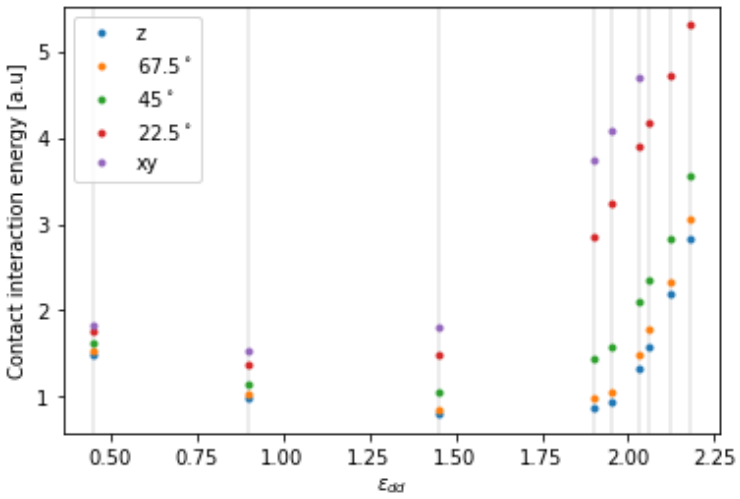

(b) Contact interaction energy ϵ_{dd}

Figure 4.9: Dipolar and contact interaction energies vs ϵ_{dd} in subfigures 4.9a and 4.9b

There are also two important differences between figures 4.9a and 4.9b:

- All contact interaction energy points are positive, whereas in the dipolar case, some are positive and some others are negative. More precisely, for orientations z and 67.5°, and until $\epsilon_{dd} = 1.95$ (right before the droplet differentiation phase), the dipolar interaction energy is positive; and in the case of 22.5°, until $\epsilon_{dd} = 0.90$ (during the tori phase). These observations might be another reason for droplet formation stages occurring at different ϵ_{dd} values, and with the gas taking slightly different, and even quite different, shapes depending on the direction of magnetisation.
- For all orientations, and at ϵ_{dd} values of 0.45, 0.90 and 1.45, the contact interaction energy seems to dominate over the dipolar one. This is consistent with the gas not being dense and going through the pancake and tori stages. However, as ϵ_{dd} increases, the attractive dipole interaction becomes stronger than the repulsive contact interaction. Although the difference between the two energies is not so notable, this means that for droplets to be fully defined and elongate, both interactions must be symmetric in the previously explained way while dipole attraction being a bit stronger than the contact repulsion.

4.2.3 Kinetic energy

Concerning the kinetic energies in figure 4.10a, although they tend to increase, they are still very small compared to the energy of the interactions. This plot can be considered a sanity check as the Thomas-Fermi regime was assumed for the derivation of the LHY-correction.

4.2.4 Ground state energy

Finally, we reach the discussion of the ground state energies in figure 4.10b. From its decreasing tendency, it can be inferred that quantum droplets are the best spatial configuration energy-wise so far for our system.

One of the most important conclusions of this thesis is that, at least, for every ϵ_{dd} considered, the ground state energy gets smaller as the orientation approaches the xy plane. In other words, xy plane orientation is the best configuration so far. However, the reasons for this are more complex than expected, and further investigation must be made.

Regarding decreasing rates, they are higher in modulus as again the orientation approaches the xy plane. However, there does not seem to be a common fast slope for the data points corresponding to the droplet differentiation phase. Moreover, at such ϵ_{dd} values, the decreasing tendency is not so strong as in figure 4.9. This could mean that quantum droplets are a more stable spacial configuration compared to the shapes of the previous phases.

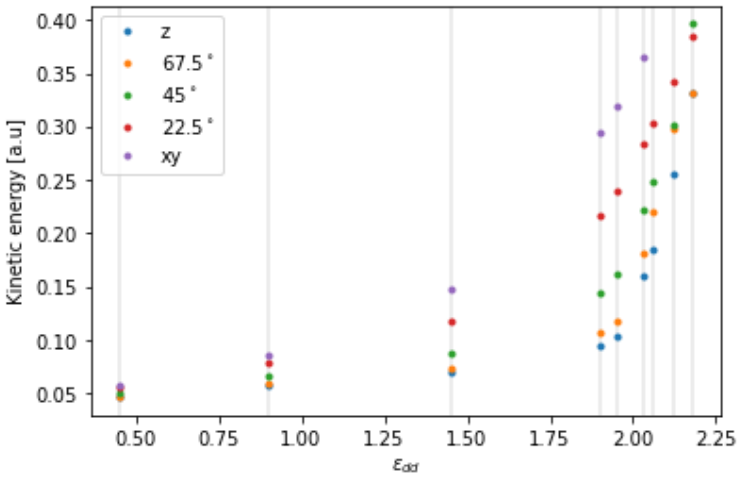

(a) Kinetic energy vs ϵ_{dd}

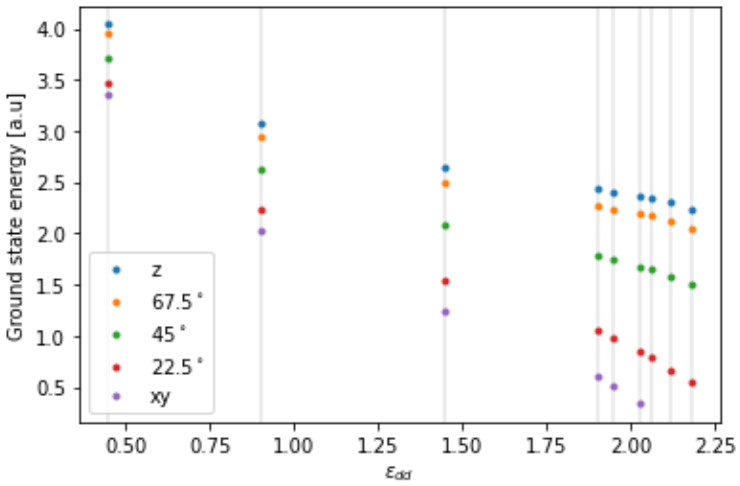

(b) Ground state energy ϵ_{dd}

Figure 4.10: Kinetic and ground state energies vs ϵ_{dd} in subfigures 4.10a and 4.10b

Finally, a coincidence that might be useful to keep in mind for future studies is that the same clustering of orientations found in figures 4.8 and 4.9b is again present here, meaning that the dipolar and contact interactions might be the most important components in the computation of the ground state energy.

Chapter 5

Conclusions and overview

Now that the results have been shown and accompanied by a discussion, it is good to recapitulate everything seen so far.

Chapter one consisted of a brief history of the study of dipolar BEC's, the topic of the thesis was introduced, and a description of the rest of the sections in this document was given. Here we have seen that the original topic was the study of supersolidity, superfluidity, droplet formation and persistent current formation of a rotating dipolar gas in [23], with the difference that this time magnetic dipole moments would have been aligned in the xy plane instead of in the z direction.
Before addressing this ambitious topic, it was necessary to study the quantum droplet formation for the case of static gas with different dipole moment orientations, from the z axis to the xy plane.
There are two reasons why finally it was not possible to go through the rotating case. The first one was because it took more time than expected for the energy values of the density plots to converge; especially for the ones in 4.7, where the last three subfigures were taking too much time and it was clear that they were going to consist on two thick, elongated droplets very similar to the three last ones obtained.
The second reason is that we had to ensure that the program was not falling into local minima when trying to compute the ground state energy for certain parameter values.
One possible way to avoid this brute force approach is to develop a genetic algorithm such that per every orientation and ϵ_{dd} value, it finds the potential guess (or guesses) leading to the true ground state energy in a more heuristic way.
In any case, it is of interest that this project continues by addressing the rotating gas case as the results might be worth comparing with the ones in [23]. As an example of next step, an interesting Master thesis could consist of trying increasing values of angular momentum for the orientations z and xy and the ϵ_{dd} values considered in this thesis. It is a good idea to prioritise the xy orientation over the remaining three ones as we have shown it is the best orientation energy-wise and again it already took more time than expected to get results.

The theory chapter started with the basic ideas about ideal BEC's, as it is the base for interacting BEC's. Subsequently, the two interactions of our system were explained, and finally, the differential equation governing the behaviour of our system was derived at the same time as a brief overview on quantum droplet formation was given.

After the theory and a brief look at the algorithm used to solve the differential equation of our system, we went through the results and discussion. Several relevant conclusions were drawn: droplets take an oval shape and are elongated in the direction of magnetisation; droplet formation is the result of a particular balance between the attractive dipolar interactions and slightly weaker repulsive interactions, where such balance seems to be the same for any orientation; finally, and probably the most important finding of this thesis, as the orientations approach the xy plane, the droplets formed have a lower ground state energy.
It is of importance to mention that we cannot rely on an analytical solution of the differential equation, as it makes the reaching of conclusions more difficult. Moreover, within the time for the thesis, it was unfeasible to

try all the possible potential guesses according to the program, but only a subset of them. This implies that the values of the energies obtained correspond to ground states with high probability. As a more optimistic comment, it is possible to overcome this last obstacle with the mentioned genetic algorithm.

Bibliography

[1] A. Einstein. Quantentheorie des einatomigen idealen Gases. In *Albert Einstein: Akademie-Vorträge*, pages 237–244. John Wiley & Sons, Ltd, (2005).

[2] A Einstein. Quantentheorie des einatomigen idealen Gases. Zweite Abhandlung. In *Albert Einstein: Akademie-Vorträge*, pages 245–257. John Wiley & Sons, Ltd, (2005).

[3] S. N. Bose. Plancks Gesetz und Lichtquantenhypothese. *Zeitschrift für Physik*, 26(1):178–181, (1924).

[4] N. Bogoliubov. On the theory of superfluidity. *Journal of Physics*, 11(1), (1947).

[5] L. Pitaevskii and S. Stringari. *Bose-Einstein Condensation and Superfluidity*. Oxford University Press, (2016).

[6] F. London. On the Bose-Einstein Condensation. *Physical Review*, 54(11):947–954, 12 (1938).

[7] L. Onsager. Statistical hydrodynamics. *Il Nuovo Cimento (1943-1954)*, 6(2):279–287, (1949).

[8] R. P. Feynman. Chapter II Application of Quantum Mechanics to Liquid Helium. In C J Gorter, editor, *Progress in Low Temperature Physics*, volume 1, pages 17–53. Elsevier, (1955).

[9] H. E. Hall and W. F. Vinen. The rotation of liquid helium II I. Experiments on the propagation of second sound in uniformly rotating helium II. *The Royal Society Mond Laboratory, University of Cambdridge*, 238(1213), (1956).

[10] M. H. Anderson, J. R. Ensher, M. R. Matthews, C. E. Wieman, and E. A. Cornell. Observation of Bose-Einstein Condensation in a Dilute Atomic Vapor. *Science*, 269(5221):198, 7 (1995).

[11] C. C. Bradley, C. A. Sackett, J. J. Tollett, and R. G. Hulet. Evidence of Bose-Einstein Condensation in an Atomic Gas with Attractive Interactions. *Physical Review Letters*, 75(9):1687–1690, 8 (1995).

[12] K. B. Davis, M. O. Mewes, M. R. Andrews, N. J. van Druten, D. S. Durfee, D. M. Kurn, and W. Ketterle. Bose-Einstein Condensation in a Gas of Sodium Atoms. *Physical Review Letters*, 75(22):3969–3973, 11 (1995).

[13] D. Boholm. Self-bound droplets in quasi two-dimensional dipole-dipole interacting bose-einstein condensates. Technical report, Lund University, 12 (2018).

[14] T. D. Lee, K. Huang, and C. N. Yang. Eigenvalues and Eigenfunctions of a Bose System of Hard Spheres and Its Low-Temperature Properties. *Physical Review*, 106(6):1135–1145, 6 (1957).

[15] D. S. Petrov. Quantum Mechanical Stabilization of a Collapsing Bose-Bose Mixture. *Physical Review Letters*, 115(15), 10 (2015).

[16] M. Schmitt, M. Wenzel, F. Böttcher, I. Ferrier-Barbut, and T. Pfau. Self-bound droplets of a dilute magnetic quantum liquid. *Nature*, 539(7628):259–262, 11 (2016).

[17] H. Kadau, M. Schmitt, M. Wenzel, C. Wink, T. Maier, I. Ferrier-Barbut, and T. Pfau. Observing the Rosensweig instability of a quantum ferrofluid. *Nature*, 530(7589):194–197, 2 (2016).

[18] I. Ferrier-Barbut, H. Kadau, M. Schmitt, M. Wenzel, and T. Pfau. Observation of Quantum Droplets in a Strongly Dipolar Bose Gas. *Physical Review Letters*, 116(21), 5 (2016).

[19] C. R. Cabrera, L. Tanzi, J. Sanz, B. Naylor, P. Thomas, P. Cheiney, and L. Tarruell. Quantum liquid droplets in a mixture of bose-einstein condensates. *Science*, 359:301–304, (2018).

[20] G. Semeghini, G. Ferioli, L. Masi, C. Mazzinghi, L. Wolswijk, F. Minardi, M. Modugno, G. Modugno, M. Inguscio, and M. Fattori. Self-Bound Quantum Droplets of Atomic Mixtures in Free Space. *Physical Review Letters*, 120(23):235301, 6 (2018).

[21] Fabian Böttcher, Jan-Niklas Schmidt, Matthias Wenzel, Jens Hertkorn, Mingyang Guo, Tim Langen, and Tilman Pfau. Transient supersolid properties in an array of dipolar quantum droplets. *Phys. Rev. X*, 9:011051, Mar 2019.

[22] P. B. Blakie, D. Baillie, L. Chomaz, and F. Ferlaino. Supersolidity in an elongated dipolar condensate. *arXiv*, 4 2020.

[23] M. Nilsson Tengstrand, D. Boholm, R. Sachdeva, J. Bengtsson, and S. M. Reimann. Persistent currents in toroidal dipolar supersolids. *Physical Review A*, 103(1), 1 (2021).

[24] M. Wenzel. *Macroscopic States of Dipolar Quantum Gases.* PhD thesis, Universität Stuttgart, 2018.

[25] T. Lahaye, C. Menotti, L. Santos, M. Lewenstein, and T. Pfau. The physics of dipolar bosonic quantum gases. *Reports on Progress in Physics*, 5 (2009).

[26] A. R.P. Lima and A. Pelster. Beyond mean-field low-lying excitations of dipolar Bose gases. *Physical Review A - Atomic, Molecular, and Optical Physics*, 86(6), 12 (2012).

[27] P. Stürmer. *Real-time stability and dynamics of vortices in quasi-two-dimensional self-bound two-component Bose-Einstein condensates.* PhD thesis, Lund Univeristy, Lund, 5 (2019).

[28] H. Bruus and K. Flensberg. *Many-body quantum theory in condensed matter physics - an introduction.* Oxford University Press, United States, (2004).

[29] P-G de. Gennes. *Superconductivity of metals and alloys.* Advanced Book Program, Perseus Books, Reading, Mass., (1999).

[30] S. Giorgini, L. P. Pitaevskii, and S. Stringari. Thermodynamics of a trapped bose-condensed gas. *Journal of Low Temperature Physics*, 109:309–355, 1997.

[31] Eddy Timmermans, Paolo Tommasini, and Kerson Huang. Variational thomas-fermi theory of a nonuniform bose condensate at zero temperature. *Phys. Rev. A*, 55:3645–3657, May 1997.

[32] Philipp Bader, Sergio Blanes, and Fernando Casas. Solving the schrödinger eigenvalue problem by the imaginary time propagation technique using splitting methods with complex coefficients. *The Journal of Chemical Physics*, 139(12):124117, 2013.

[33] Z. Kuhrij. *Motion of a Gaussian Through a 2D Dilute BEC.* PhD thesis, Lund University, 5 (2020).

[34] M. Aichinger, S. A. Chin, and E. Krotscheck. Fourth-order algorithms for solving local Schrödinger equations in a strong magnetic field. *Computer Physics Communications*, 171(3):197–207, 10 (2005).

[35] S. A. Chin and E. Krotscheck. Fourth-order algorithms for solving the imaginary-time Gross-Pitaevskii equation in a rotating anisotropic trap. *Physical Review E - Statistical, Nonlinear, and Soft Matter Physics*, 72(3), 9 (2005).

Annexe

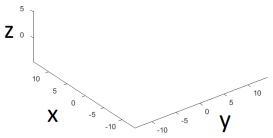

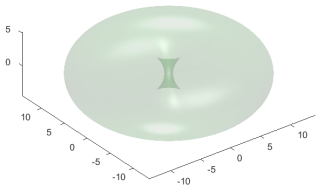

(a) $\epsilon_{dd} = 0.45$

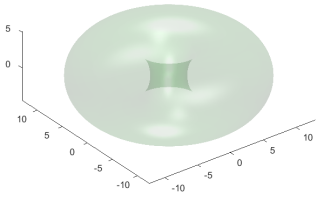

(b) $\epsilon_{dd} = 0.90$

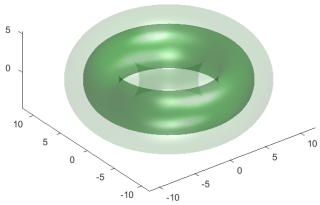

(c) $\epsilon_{dd} = 1.45$

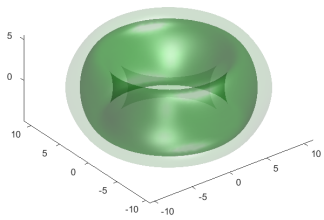

(d) $\epsilon_{dd} = 1.90$

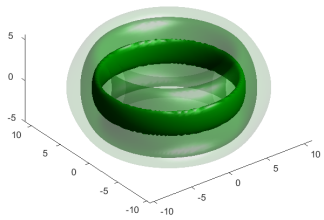

(e) $\epsilon_{dd} = 1.95$

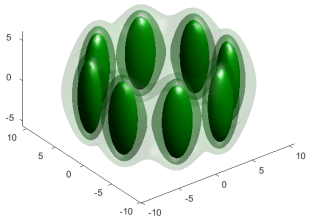

(f) $\epsilon_{dd} = 2.03$

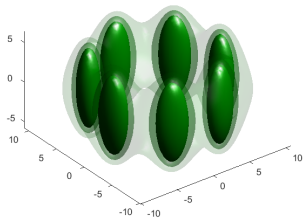

(g) $\epsilon_{dd} = 2.06$

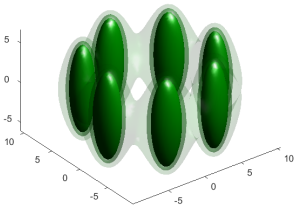

(h) $\epsilon_{dd} = 2.12$

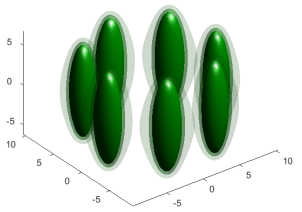

(i) $\epsilon_{dd} = 2.18$

Figure 5.1: Formation of droplets as ϵ_{dd} increases with magnetic dipole moments in the z direction. All subfigures were generated by using a mesh size of 7, an imaginary step size of 0.005 and contour densities $0.8 \cdot 10^{-3}, 0.4 \cdot 10^{-3}$ and $0.1 \cdot 10^{-3}$. The separate subfigure in the first row shows the axis convention followed by the rest of the subfigures in this document.

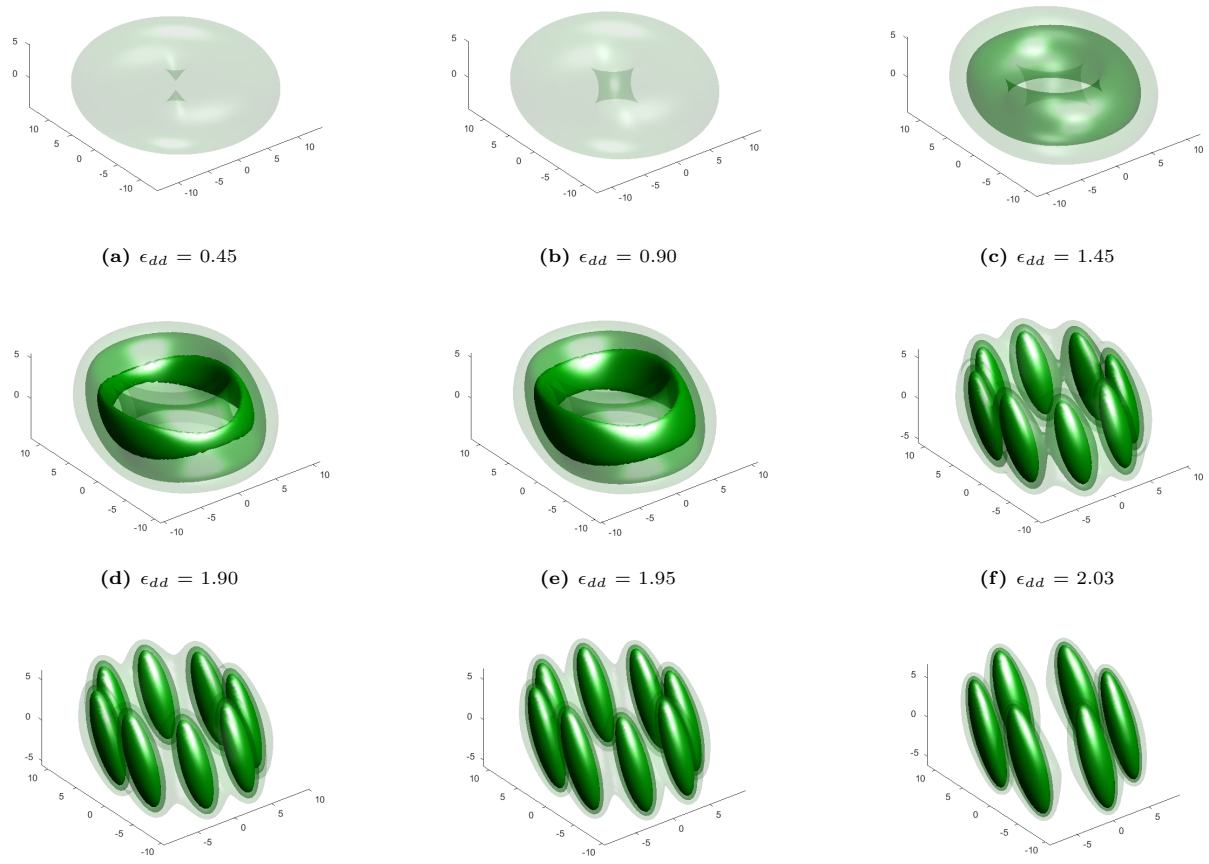

(a) $\epsilon_{dd} = 0.45$ **(b)** $\epsilon_{dd} = 0.90$ **(c)** $\epsilon_{dd} = 1.45$

(d) $\epsilon_{dd} = 1.90$ **(e)** $\epsilon_{dd} = 1.95$ **(f)** $\epsilon_{dd} = 2.03$

(g) $\epsilon_{dd} = 2.06$ **(h)** $\epsilon_{dd} = 2.12$ **(i)** $\epsilon_{dd} = 2.18$

Figure 5.2: Formation of droplets as ϵ_{dd} increases with magnetic dipole moments at 67.5° form the $x-y$ plane. All subfigures were generated by using a mesh size of 7, an imaginary step size of 0.005 and contour densities $0.8 \cdot 10^{-3}, 0.4 \cdot 10^{-3}$ and $0.1 \cdot 10^{-3}$.

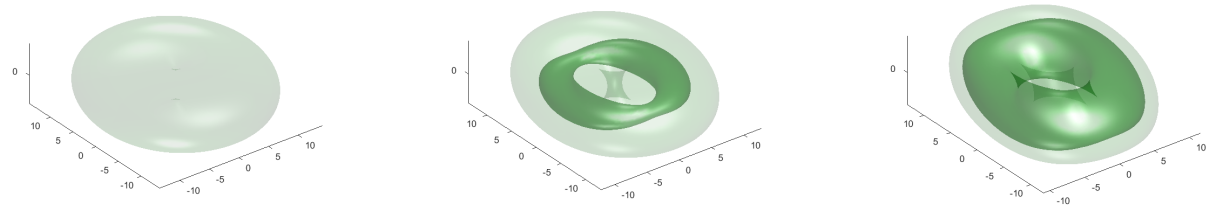

(a) $\epsilon_{dd} = 0.45$ **(b)** $\epsilon_{dd} = 0.90$ **(c)** $\epsilon_{dd} = 1.45$

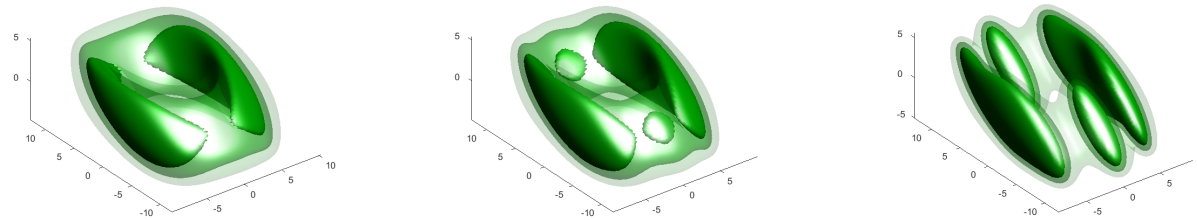

(d) $\epsilon_{dd} = 1.90$ **(e)** $\epsilon_{dd} = 1.95$ **(f)** $\epsilon_{dd} = 2.03$

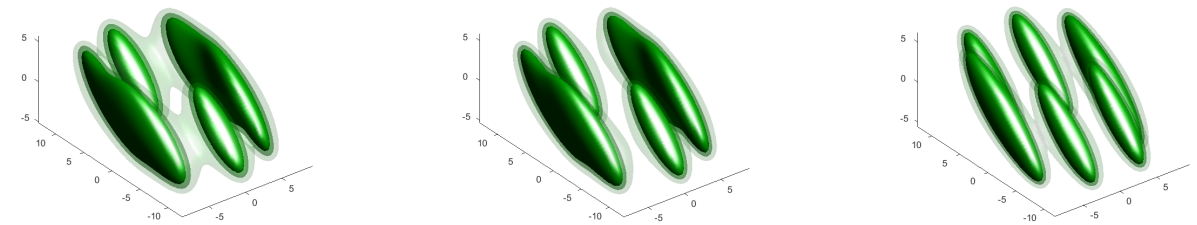

(g) $\epsilon_{dd} = 2.06$ **(h)** $\epsilon_{dd} = 2.12$ **(i)** $\epsilon_{dd} = 2.18$

Figure 5.3: Formation of droplets as ϵ_{dd} increases with magnetic dipole moments at 45° form the $x - y$ plane. All subfigures were generated by using a mesh size of 7, an imaginary step size of 0.005 and contour densities $0.8 \cdot 10^{-3}, 0.4 \cdot 10^{-3}$ and $0.1 \cdot 10^{-3}$.

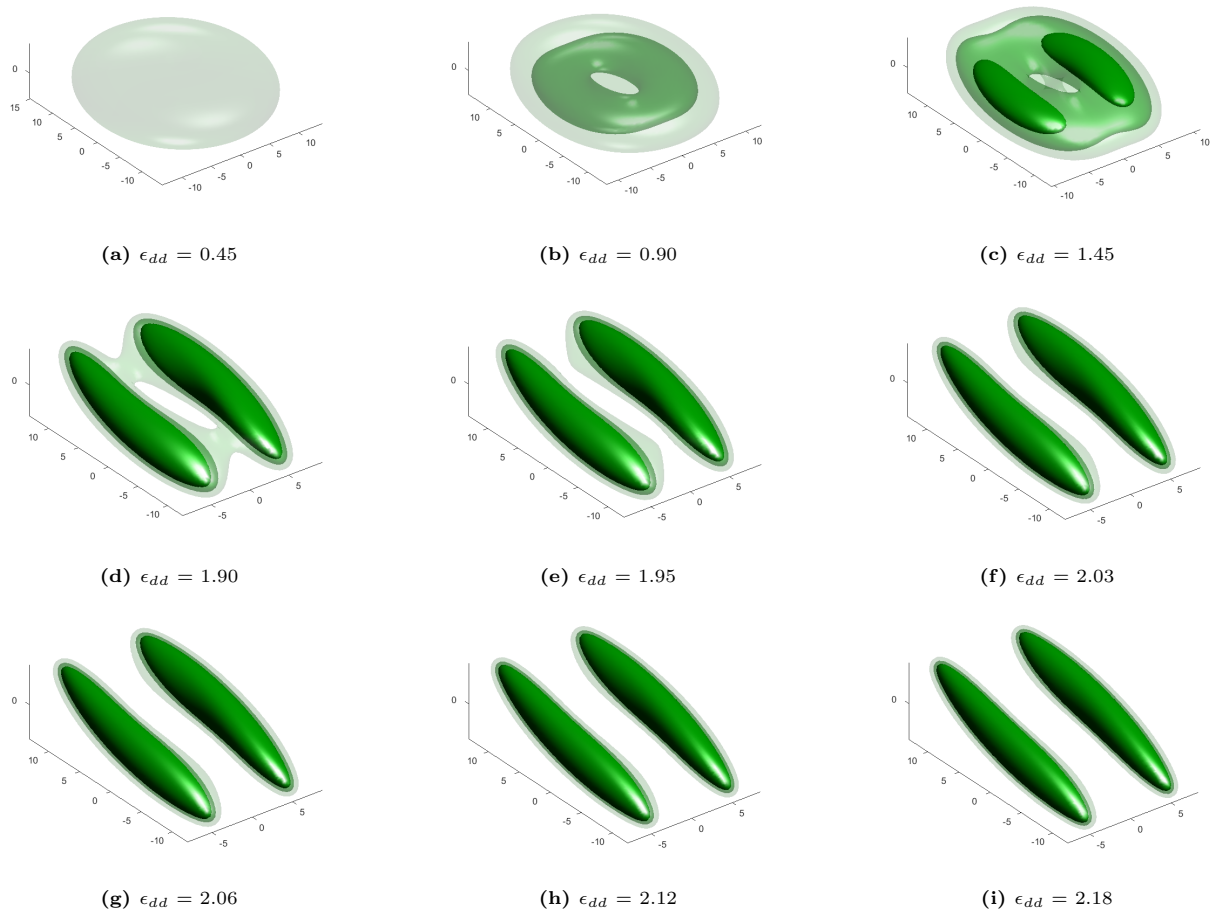

(a) $\epsilon_{dd} = 0.45$ **(b)** $\epsilon_{dd} = 0.90$ **(c)** $\epsilon_{dd} = 1.45$

(d) $\epsilon_{dd} = 1.90$ **(e)** $\epsilon_{dd} = 1.95$ **(f)** $\epsilon_{dd} = 2.03$

(g) $\epsilon_{dd} = 2.06$ **(h)** $\epsilon_{dd} = 2.12$ **(i)** $\epsilon_{dd} = 2.18$

Figure 5.4: Formation of droplets as ϵ_{dd} increases with magnetic dipole moments at 22.5° form the $x-y$ plane. All subfigures were generated by using a mesh size of 7, an imaginary step size of 0.005 and contour densities $0.8 \cdot 10^{-3}, 0.4 \cdot 10^{-3}$ and $0.1 \cdot 10^{-3}$.

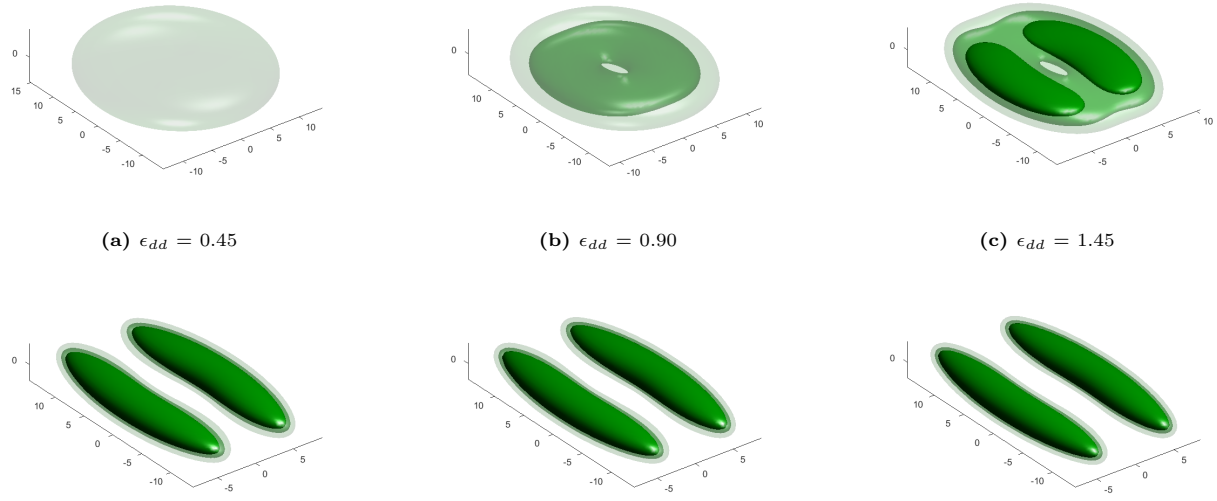

(a) $\epsilon_{dd} = 0.45$ **(b)** $\epsilon_{dd} = 0.90$ **(c)** $\epsilon_{dd} = 1.45$

(d) $\epsilon_{dd} = 1.90$ **(e)** $\epsilon_{dd} = 1.95$ **(f)** $\epsilon_{dd} = 2.03$

Figure 5.5: Formation of droplets as ϵ_{dd} increases with magnetic dipole moments in the $x - y$ plane. All subfigures were generated by using a mesh size of 7, an imaginary step size of 0.005 and contour densities $0.8 \cdot 10^{-3}, 0.4 \cdot 10^{-3}$ and $0.1 \cdot 10^{-3}$.